

Measurements of the Rate of Type Ia Supernovae at Redshift $\lesssim 0.3$ from the SDSS-II Supernova Survey

bdilday@physics.rutgers.edu

Benjamin Dilday,^{1,2,3} Mathew Smith,^{4,5} Bruce Bassett,^{4,6} Andrew Becker,⁷ Ralf Bender,^{8,9} Francisco Castander,¹⁰ David Cinabro,¹¹ Alexei V. Filippenko,¹² Joshua A. Frieman,^{13,14} Lluís Galbany,¹⁵ Peter M. Garnavich,¹⁶ Ariel Goobar,^{17,18} Ulrich Hopp,^{8,9} Yutaka Ihara,¹⁹ Saurabh W. Jha,¹ Richard Kessler,^{3,13} Hubert Lampeitl,⁵ John Marriner,¹⁴ Ramon Miquel,^{15,20} Mercedes Mollá,²¹ Robert C. Nichol,⁵ Jakob Nordin,¹⁸ Adam G. Riess,^{22,23} Masao Sako,²⁴ Donald P. Schneider,²⁵ Jesper Sollerman,^{17,26} J. Craig Wheeler,²⁷ Linda Östman,¹⁸ Dmitry Bizyaev,²⁸ Howard Brewington,²⁸ Elena Malanushenko,²⁸ Viktor Malanushenko,²⁸ Dan Oravetz,²⁸ Kaike Pan,²⁸ Audrey Simmons,²⁸ and Stephanie Snedden²⁸

¹ Department of Physics and Astronomy, Rutgers, the State University of New Jersey, 136 Frelinghuysen Rd., Piscataway, NJ 08854.

² Department of Physics, University of Chicago, Chicago, IL 60637.

³ Kavli Institute for Cosmological Physics, The University of Chicago, 5640 South Ellis Ave., Chicago, IL 60637.

⁴ Department of Mathematics and Applied Mathematics, University of Cape Town, Rondebosch 7701, South Africa.

⁵ Institute of Cosmology and Gravitation, Mercantile House, Hampshire Terrace, University of Portsmouth, Portsmouth PO1 2EG, United Kingdom.

⁶ South African Astronomical Observatory, P.O. Box 9, Observatory 7935, South Africa.

⁷ Department of Astronomy, University of Washington, Box 351580, Seattle, WA 98195.

⁸ Max Planck Institute for Extraterrestrial Physics, D-85748 Garching, Germany.

⁹ Universitaets-Sternwarte Munich, 1 Scheinerstrasse, D-81679 Munich, Germany.

¹⁰ Institut de Ciències de l’Espai (IEEC-CSIC), Barcelona, Spain.

¹¹ Department of Physics and Astronomy, Wayne State University, Detroit, MI 48202.

¹² Department of Astronomy, University of California, Berkeley, CA 94720-3411.

¹³ Department of Astronomy and Astrophysics, The University of Chicago, 5640 South Ellis Avenue, Chicago, IL 60637.

¹⁴ Center for Astrophysics, Fermi National Accelerator Laboratory, P.O. Box 500, Batavia, IL 60510.

¹⁵ Institut de Física d’Altes Energies, Barcelona, Spain.

¹⁶ University of Notre Dame, 225 Nieuwland Science, Notre Dame, IN 46556-5670.

¹⁷ The Oskar Klein Centre, Department of Astronomy, Albanova, Stockholm University, SE-106 91 Stockholm, Sweden.

¹⁸ Department of Physics, Stockholm University, Albanova University Center, S-106 91 Stockholm, Sweden.

¹⁹ Institute of Astronomy, Graduate School of Science, University of Tokyo 2-21-1, Osawa, Mitaka, Tokyo 181-0015, Japan.

²⁰ Institució Catalana de Recerca i Estudis Avançats, Barcelona, Spain.

²¹ Centro de Investigaciones Energéticas, Medioambientales y Tecnológicas, Madrid, Spain.

²² Space Telescope Science Institute, 3700 San Martin Drive, Baltimore, MD 21218.

²³ Department of Physics and Astronomy, Johns Hopkins University, 3400 North Charles Street, Baltimore, MD 21218.

²⁴ Department of Physics and Astronomy, University of Pennsylvania, 209 South 33rd Street, Philadelphia,

January 27, 2010

ABSTRACT

We present a measurement of the volumetric Type Ia supernova (SN Ia) rate based on data from the Sloan Digital Sky Survey II (SDSS-II) Supernova Survey. The adopted sample of supernovae (SNe) includes 516 SNe Ia at redshift $z \lesssim 0.3$, of which 270 (52%) are spectroscopically identified as SNe Ia. The remaining 246 SNe Ia were identified through their light curves; 113 of these objects have spectroscopic redshifts from spectra of their host galaxy, and 133 have photometric redshifts estimated from the SN light curves. Based on consideration of 87 spectroscopically confirmed non-Ia SNe discovered by the SDSS-II SN Survey, we estimate that $2.04^{+1.61}_{-0.95}\%$ of the photometric SNe Ia may be misidentified. The sample of SNe Ia used in this measurement represents an order of magnitude increase in the statistics for SN Ia rate measurements in the redshift range covered by the SDSS-II Supernova Survey. If we assume a SN Ia rate that is constant at low redshift ($z < 0.15$), then the SN observations can be used to infer a value of the SN rate of $r_V = (2.69^{+0.34+0.21}_{-0.30-0.01}) \times 10^{-5}$ SNe yr $^{-1}$ Mpc $^{-3}$ ($H_0/(70 \text{ km s}^{-1} \text{ Mpc}^{-1})^3$) at a mean redshift of ~ 0.12 , based on 79 SNe Ia of which 72 are spectroscopically confirmed. However, the large sample of SNe Ia included in this study allows us to place constraints on the redshift dependence of the SN Ia rate based on the SDSS-II Supernova Survey data alone. Fitting a power-law model of the SN rate evolution, $r_V(z) = A_p \times ((1+z)/(1+z_0))^\nu$, over the redshift range $0.0 < z < 0.3$ with $z_0 = 0.21$, results in $A_p = (3.43^{+0.15}_{-0.15}) \times 10^{-5}$ SNe yr $^{-1}$ Mpc $^{-3}$ ($H_0/(70 \text{ km s}^{-1} \text{ Mpc}^{-1})^3$) and $\nu = 2.04^{+0.90}_{-0.89}$.

Subject headings: supernovae: general — supernovae: rates

PA 19104.

²⁵ Department of Astronomy and Astrophysics, 525 Davey Laboratory, Pennsylvania State University, University Park, PA 16802.

²⁶ Dark Cosmology Centre, Niels Bohr Institute, University of Copenhagen, Denmark.

²⁷ Department of Astronomy, University of Texas, Austin, TX 78712.

²⁸ Apache Point Observatory, P.O. Box 59, Sunspot, NM 88349.

1. Introduction

Type Ia supernovae (SNe Ia) occupy a prominent position in contemporary astrophysics, in part due to their utility as cosmological distance indicators (for a review, see Filippenko 2005). The observed correlation between the peak luminosity and the rate of decline for SNe Ia (Pskovskii 1977; Phillips 1993) has been exploited to improve the accuracy of measured distances to SNe Ia and thereby place important constraints on cosmological models (e.g., Riess et al. 1998; Perlmutter et al. 1999; Riess et al. 2004; Astier et al. 2006; Wood-Vasey et al. 2007; Riess et al. 2007; Hicken et al. 2009; Riess et al. 2009; Freedman et al. 2009; Kessler et al. 2009). However, the SN Ia decline rate vs. peak luminosity correlation is mainly an empirically determined phenomenon, and the exact nature of the progenitor systems that give rise to SNe Ia remains uncertain. A better understanding of SN Ia progenitor systems is desirable both for investigations of fundamental astrophysics (e.g., binary star evolution and explosion physics) and to provide a theoretical foundation for understanding any possible evolution of SN Ia properties (such as the decline rate vs. peak luminosity correlation) with redshift that could cause additional systematic effects in distance measurements.

The SN Ia rate can be used to place important constraints on the progenitor systems of SNe Ia. In general, the SN Ia rate can be expressed as a delay function convolved with the cosmic star-formation rate (SFR) (e.g., Greggio 2005). That is,

$$r(t) = \int_0^t k_{\Gamma}(t') \Psi(t') A_{\text{SN}}(t-t') D(t-t') dt', \quad (1)$$

where $r(t)$ is the SN rate, $\Psi(t')$ is the SFR, $k_{\Gamma}(t')$ is the number of stars per unit mass for the population formed at epoch t' , $A_{\text{SN}}(t-t')$ is the number of stars from the population that will result in SN explosions, and $D(t-t')$ is a distribution of delay times between the formation of a stellar system and the resulting SN explosion. The delay function varies depending on the model assumed for the progenitors of SNe Ia, and measurements of the SN rate, in combination with measurements of the cosmic SFR, can therefore place observational constraints on SN Ia progenitor models. We emphasize that according to Eq. (1), constraints on SN Ia progenitor systems rely not only on precise measurements of the SN rate, but also on measurements of the cosmic SFR. At present, measurements of the cosmic SFR (as a function of time) suffer from significant uncertainties, thus complicating the interpretation of the cosmic SN rate in terms of delay functions (Förster et al. 2006). In this paper, we focus on presenting our SN rate measurements and will not pursue detailed comparisons to the cosmic SFR.

The SN rate was first measured by Zwicky (1938), who found it to be approximately “one SN per few hundred years per average nebula,” in the local universe. Subsequently, improvements in astronomical technology as well as increased observing time dedicated to SN searches have led to more precise SN rate measurements, spanning a wide range of redshifts. In the local universe, the SN Ia rate has been measured by Cappellaro et al. (1999) from ~ 140 SNe Ia and by Li et al. (2010a,b) from ~ 930 SNe Ia. At intermediate redshifts ($0.1 \lesssim z \lesssim 0.5$), the SN Ia rate has been measured by many authors (e.g., Hardin et al. 2000; Pain et al. 2002; Madgwick et al. 2003; Tonry et al. 2003; Blanc et al. 2004; Neill et al. 2006; Sullivan et al. 2006b; Botticella et al. 2008). At high redshifts, the SN Ia rate has been measured with data from the *Hubble Space Telescope (HST)* by Dahlen et al. (2004, 2008). All of these SN rate measurements are based on SN Ia samples that are primarily spectroscopically identified and were determined in a manner similar to that of the SDSS-II Supernova Survey SN rate analysis presented here. In addition to these measurements, a number of authors have presented SN Ia rate analyses based on photometric identification of SNe Ia, in many cases with only a few photometric observations. These include measurement of the intermediate-redshift rate by Horesh et al. (2008), the intermediate-to-high redshift rate by Barris & Tonry (2006), and the high-redshift rate by Poznanski et al. (2007) and Kuznetsova et al. (2008).

A precise measurement of the low-redshift ($z < 0.12$) SN Ia rate, based on 17 SNe Ia from the first season of the SDSS-II Supernova Survey, was given by Dilday et al. (2008). In the present paper we discuss an extension of this volumetric SN Ia rate measurement to a higher redshift limit, based on all three seasons of the SDSS-II Supernova Survey (Frieman et al. 2008). Including SNe from three years of the SDSS-II Supernova Survey and considering a larger redshift range results in a major increase in the number of SNe used for the rate measurement. At low redshifts, the SN rate measurements discussed here have the same high purity and completeness as for the low-redshift rate from the first season discussed by Dilday et al. (2008), but with increased statistical power. Inclusion of higher-redshift SNe allows for investigation of the redshift dependence of the SN Ia rate over the range covered by the SDSS-II Supernova Survey. However, at higher redshifts, systematic uncertainties become increasingly important and eventually dominate the error budget. The efficiency studies and SN selection functions described herein have also been used to estimate the SN Ia rate as an explicit function of the properties of their host galaxies (Smith et al. 2010) and for studies of the SN Ia rate in clusters of galaxies (Dilday et al. 2010).

The rest of this paper is organized as follows. In §2 we briefly describe the observations and SN search strategy of the SDSS-II Supernova Survey. Section 3 discusses selection of the SN rate sample from the SDSS-II Supernova Survey data, and §4 determines the efficiency for SN selection. We present our measurement of the SN Ia rate in §5, and our conclusions

are summarized in §6. Whenever necessary, we assume a flat Λ CDM universe with $\Omega_m = 0.3$, $\Omega_\Lambda = 0.7$, and $H_0 = 70 \text{ km s}^{-1} \text{ Mpc}^{-1}$.

2. SDSS-II Supernova Survey Observations

Here we briefly describe aspects of the SDSS-II Supernova Survey most relevant to the present SN rate analysis. Much of the material in this section is also relevant to the SN rate studies described by Dilday et al. (2010), and is discussed more fully therein. The survey is described in more detail by Frieman et al. (2008), and the SN detection algorithms are given by Sako et al. (2008). Additional details of the survey observations and the use of *in situ* artificial SNe for determining SN detection efficiencies are discussed by Dilday et al. (2008). A technical summary of the SDSS is given by York et al. (2000). Details of the survey calibration are provided by Hogg et al. (2001), Smith et al. (2002), and Tucker et al. (2006). The data processing and quality assessment are discussed by Ivezić et al. (2004), and the photometric pipeline is described by Lupton et al. (1999).

The SDSS-II Supernova Survey was carried out during the Fall (September–November) of 2005–2007, using the 2.5 m telescope (Gunn et al. 2006) at Apache Point Observatory (Sacramento Peak, New Mexico). Observations were obtained in the SDSS *ugriz* filters (Fukugita et al. 1996) with a wide-field CCD camera (Gunn et al. 1998), operating in time-delay-and-integrate (TDI, or drift scan) mode. The region of the sky covered by the SDSS-II Supernova Survey (designated Stripe 82; see Stoughton et al. 2002) was bounded by $-60^\circ < \alpha_{J2000} < 60^\circ$ and $-1.258^\circ < \delta_{J2000} < 1.258^\circ$. On average, any given part of this ~ 300 square degree area was imaged once every 4 days during the survey operations.

Difference images were produced in the SDSS *gri* filter bands by subtracting template images, constructed from previous survey observations of the region, using an implementation of the methods described by Alard & Lupton (1998). The difference images were searched for positive fluctuations using the DoPHOT photometry and object detection package (Schechter et al. 1993); typical limits (10σ above background) for the SDSS-II Supernova Survey were $g \approx 21.8$, $r \approx 21.5$, and $i \approx 21.2$ mag. A combination of software cuts and human visual inspection was then used to identify promising SN candidates from the full set of transient detections. As a key component of prioritizing SN candidates for follow-up spectroscopic observations, the light curves of SN candidates were fit to models of Type Ia, Type Ib/c, and Type II SNe (see Filippenko 1997 for a review of SN types). This procedure is referred to as “photometric typing,” and is described in detail by Sako et al. (2008).

Spectroscopic observations for both SN classification and redshift determination were

provided by a number of different telescopes. The spectra of the SNe utilized in the present SN rate analysis were provided by the Hobby-Eberly 9.2 m at McDonald Observatory, the Astrophysical Research Consortium 3.5 m at Apache Point Observatory, the Hiltner 2.4 m at the Michigan-Dartmouth-MIT Observatory, the Subaru 8.2 m at the National Astronomical Observatory of Japan, the Keck-I 10 m at the W. M. Keck Observatory, the Mayall 3.8 m at Kitt Peak National Observatory, the 3.5 m ESO New Technology Telescope (NTT) at the European Southern Observatory, the SALT 11 m (9.5 m clear aperture) at the South African Astronomical Observatory, and the 2.6 m Nordic Optical Telescope, 3.5 m Telescopio Nazionale Galileo, and 4.2 m William Herschel Telescope at the Observatorio del Roque de los Muchachos. Details of the SDSS-II Supernova Survey spectroscopic data reductions are given by Zheng et al. (2008). Comparison to high-quality SDSS galaxy spectra shows that SN spectroscopic redshifts are accurate to ~ 0.0005 when galaxy emission features are used and to ~ 0.005 when SN features are used. In either case, the uncertainties in the spectroscopic SN redshifts are negligible for the SN-rate studies considered here.

While the difference imaging pipeline used during the SN search provides initial photometric measurements, subsequent to the search more precise SN photometry is provided using a scene modeling photometry (SMP) technique developed by Holtzman et al. (2008). The final analysis of SN light curves and the selection cuts used to define the SN rate sample discussed in this paper are based on SMP.

3. SN Ia Sample for the Rate Measurement

3.1. SN Selection Requirements

For the SDSS-II Supernova Survey measurement of the low-redshift SN Ia rate (Dilday et al. 2008), we included in the SN Ia sample all spectroscopically confirmed SNe Ia at $z < 0.12$, subject to a set of objective selection criteria that can be robustly modeled with our SN Monte Carlo (MC) simulations. To account for spectroscopic incompleteness, we used the MLCS2k2 SN Ia model (Jha et al. 2007) to analyze the SMP (§2) light curves for a set of ~ 1000 photometric SN candidates, which comprised ~ 500 “best” SN Ia candidates and ~ 500 randomly chosen SN candidates.

In the present analysis, we adopt a somewhat different approach to selecting the SN sample for use in measurement of the SN rate. Rather than focusing on the low-redshift ($z < 0.12$) SNe, which can be demonstrated to be a complete sample, we define objective selection criteria for SNe Ia at all redshifts, and determine the completeness of the resulting samples based on analysis of simulated samples of SNe. As discussed in §2, during the survey

the search-photometry light curves of SN candidates were fit to models of Type Ia, Type Ib/c, and Type II SNe, and the results were used as a factor in prioritizing our spectroscopic follow-up resources.

In addition, as a method of searching for photometric SNe Ia subsequent to the survey, the search-photometry light curves were used to define a Bayesian probability for each SN candidate to be a SN of a given type. This was done by marginalizing over the light-curve fit parameters to obtain the *Bayesian evidence* and requiring that the evidence for the three SN types sums to 1. This defines the “probability,” p_T , for an object to be a SN of type T. This quantity can be considered a probability in the sense that it is bounded by $0 < p_T < 1$, and is normalized to 1 ($\sum_T p_T = 1$). However, this procedure makes the initial assumption that the object is a SN (i.e., that the three types T = Ia, Ib/c, II are exhaustive), and does not allow for other possibilities for the identity of the object (e.g., active galactic nucleus). Despite this caveat, the quantities p_T are useful statistics for analyzing the search photometry light curves. The procedure is motivated by, and modeled after, that discussed by Kuznetsova & Connolly (2007) and Poznanski et al. (2007).

The selection criteria for SN candidates that we impose on the photometric-typing fits (§2) to the search photometry light curves are as follows:

1. Bayesian $p_{\text{Ia}} > 0.45$.
2. At least three search-discovery epochs.
3. If the candidate has more than five search-photometry epochs, the best-fit SN Ia model is not SN 2005gj.

These selection criteria were determined by correlating the fit results from the full analysis of the SMP light curves for the ~ 1000 photometric SN candidates from the 2005 season with statistics of the corresponding photometric-typing fits to the search photometry, and looking for a combination of cuts that would result in a sample of SN candidates with high purity and completeness with respect to SNe Ia. Several possible statistics of the photometric-typing fits were considered to see whether they would improve the efficiency for selecting SNe Ia from the search-photometry SN candidates. The conclusion of these correlation studies was that the Bayesian probability, p_{Ia} , is the best single quantity to consider for selecting a large fraction of SNe Ia, and no significant improvement was found by considering additional fit statistics, such as the value of the reduced χ^2 statistic for the fit.

The peculiar SN Ia 2005gj, which has a flat light curve after maximum brightness (Aldering et al. 2006; Prieto et al. 2007), is included as one of the SN Ia light-curve models

in the photometric-typing fits. The requirement that the best-fit SN *not* be SN 2005gj is effectively intended to remove both peculiar SNe Ia and other non-SN transients, such as active galactic nuclei. Some core-collapse SNe are well fit by the broad light curve of SN 2005gj, and this cut also serves as a way for rejecting these from our SN Ia sample selection. Search-discovery epochs refer to epochs for which the transient object was detected by the survey difference imaging and object detection pipeline (Sako et al. 2008).

This sample selection, based on the photometric-typing procedure, resulted in ~ 600 SN Ia candidates per observing season of the SDSS-II Supernova Survey. Scene modeling photometry was then generated for these candidates, producing more reliable photometry and providing measurements at additional observing epochs, compared with the SN search photometry. In addition to the requirements on the photometric-typing fits, we require the SMP light curves for the candidates to satisfy similar selection criteria on light-curve sampling and fit quality to those discussed by Dilday et al. (2008). We list these criteria below:

1. $-51^\circ < \alpha_{\text{J2000}} < 57^\circ$.
2. There are photometric observations on at least five separate epochs between -20 days and $+60$ days relative to B -band peak light in the SN rest frame.
3. At least one epoch with signal-to-noise ratio > 5 in each of g , r , and i (not necessarily the same epoch in each passband).
4. At least one photometric observation at least two days *before* B -band peak light in the SN rest frame.
5. At least one photometric observation at least ten days *after* B -band peak light in the SN rest frame.
6. MLCS2k2 light-curve fit probability > 0.001 .
7. MLCS2k2 light-curve fit parameter $\Delta > -0.4$.

The first requirement states that the SN is within the right-ascension range of the calibration-star catalog. The second and third requirements ensure that the object is a significant and authentic astrophysical transient. The fourth and fifth requirements are imposed so that we have a robust measurement of the time of maximum brightness for the SN candidates as well as a reliable measurement of the light-curve decline, which is useful for rejecting Type II SNe. The sixth requirement is used to reject peculiar SNe Ia that are not well represented

by the MLCS2k2 light-curve model, as well as non-SN Ia transient objects. The seventh requirement is additionally used to reject objects with flat light curves such as SNe II and active galactic nuclei. The low-redshift SN data used to define the MLCS2k2 model only exhibit values of the light-curve shape parameter $\Delta \gtrsim -0.35$, so a cut at $\Delta > -0.4$ specifies that the object is within the valid range of the MLCS2k2 model, with some allowance for measurement error.

3.2. SN Sample

Over the entire redshift range of SNe discovered by the SDSS-II Supernova Survey ($z \lesssim 0.45$), there are 774 SN Ia candidates (312 spectroscopically confirmed) that satisfy the selection criteria above. The redshift distribution for these SNe is shown in Figure 1. However, as will be discussed in §4, the systematic uncertainty related to our sample selection becomes dominant for $z \gtrsim 0.2$, thereby reducing our ability for making precise SN Ia rate measurements. The numbers of SNe for several values of the maximum redshift are given in Table 1. Spectroscopically confirmed SNe Ia from this sample are listed in Table 2.

SNe for which we have photometric observations of the light curve, but do not have any spectroscopic observations to determine the spectral type of the SN, are referred to as *photometric SNe*. Photometric SNe fall into two classes: (i) those that have a precisely (i.e., spectroscopically) measured redshift for their host galaxy, and (ii) those that do not have a precisely measured redshift for their host galaxy. When the redshift for a photometric SN candidate is unknown, the candidate light curve is analyzed with the “photo- z ” option in the flux-based MLCS2k2 light-curve fitter (Dilday et al. 2008). To fit SN light curves for redshift, we assume a cosmological model, and hence a distance-vs.-redshift relation, in order to take advantage of knowledge of the absolute magnitude of SNe Ia. In addition to redshift, the SN light curves are fit for the time of maximum (in the SN rest-frame B band), the luminosity parameter Δ , and the extinction parameter A_V ; see Jha et al. (2007) for a comprehensive discussion of MLCS2k2.

To investigate the accuracy and precision of the photo- z fits, we carry out photo- z fits to the spectroscopically confirmed SNe Ia, as well as to the photometric SNe Ia *with* spectroscopically measured redshifts of $z < 0.15$. At such low redshifts, this is essentially a complete sample of SNe Ia. A plot of the residuals for the photometric redshifts is shown in Figure 2, illustrating that the SN photo- z fits are negligibly biased, and accurate to ~ 0.01 at low redshift. The numbers of SNe from categories (i) and (ii) that satisfy the selection criteria are given, for several values of limiting redshift, in Table 1. Photometric SNe from categories (i) and (ii) are listed in Table 3 and Table 4, respectively.

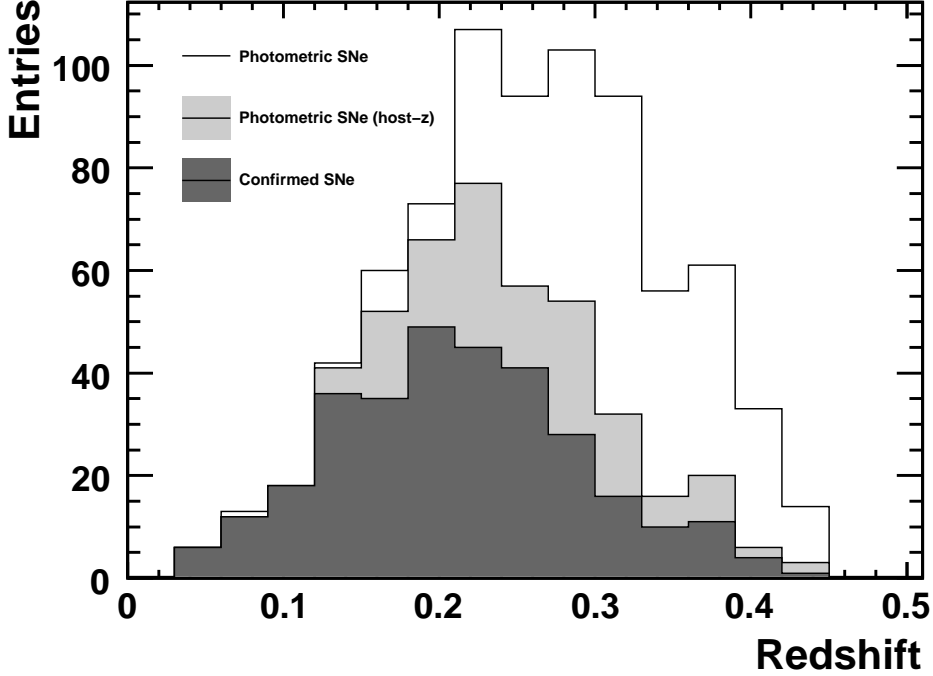


Fig. 1.— The redshift distribution for the 774 SDSS-II Supernova Survey SNe *passing* all selection criteria. The dark gray, light gray, and white shading represent spectroscopically confirmed SNe Ia, photometric SNe *with* measured host-galaxy redshifts, and photometric SNe *without* measured host-galaxy redshifts, respectively.

3.3. Bias Correction for the Observed Redshift Distribution

The observed redshift distributions for the SNe Ia from the SDSS-II Supernova Survey that satisfy the selection criteria of §3.1 are shown in Figure 1. As the number distribution is not constant with redshift, nonzero measurement error of the redshifts will result in a bias in the measured number distribution. In general, the observed number distribution as a function of redshift, $\eta(z)$, is related to the true redshift distribution, $\eta_0(z)$, through

$$\eta(z) = \int_{-\infty}^{\infty} \eta_0(z') p(z|z') dz', \quad (2)$$

where $p(z|z')$ is the probability that a SN at redshift z' will have a measured redshift of z . The number distribution, $\eta_0(z)$, is related to the volumetric rate, $r_V(z)$, and the redshift dependent efficiency, $\epsilon(z)$, through

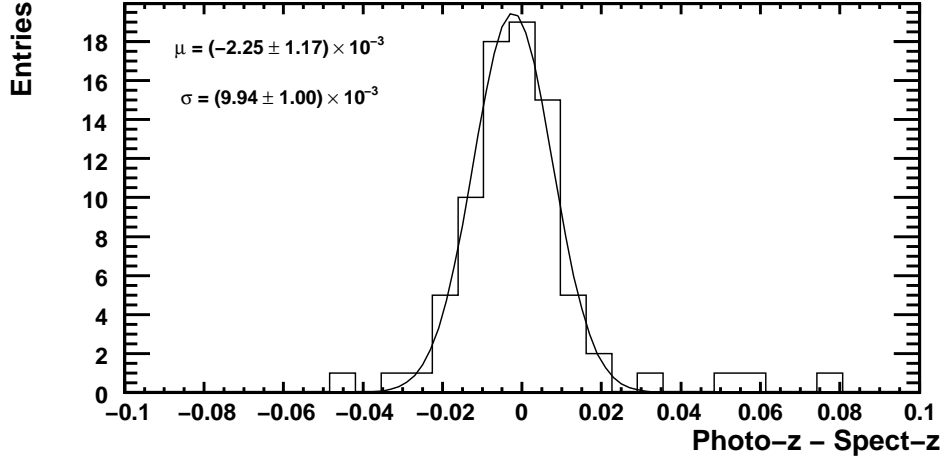


Fig. 2.— Redshift residuals (photo- z minus spectroscopic- z) for photo- z fits to a sample of spectroscopically confirmed SNe Ia and photometric SNe Ia *with* spectroscopic redshifts at $z < 0.15$. The best-fit Gaussian function is overlayed. Here, μ refers to the mean and σ to the standard deviation of the best-fit function. This plot illustrates that the SN photo- z fits are negligibly biased, and accurate to ~ 0.01 at low redshift.

$$\eta_0(z) dz \propto \frac{r_V(z) \epsilon(z)}{1+z} \frac{dV}{dz} dz, \quad (3)$$

where dV/dz is the volume element at redshift z . In what follows, we use a Gaussian approximation for $p(z|z')$, which in most cases is a good representation of the SDSS-SN photo- z errors,

$$p(z|z') = \frac{1}{\sqrt{2\pi}\sigma(z')} e^{-(z-z')^2/2\sigma^2(z')}, \quad (4)$$

where $\sigma(z')$ is the standard deviation of the SN photo- z . To determine $\sigma(z')$, we perform photo- z fits for all SNe that pass our selection criteria and then fit a power law for the typical error in the photo- z . The photo- z error as a function of fitted photo- z is shown in Figure 3, along with the best-fit power law, $\sigma(z) = A z^k$. The best fit has $A \approx 0.2$ and $k \approx 1.5$.

To estimate the bias in the observed SN number distribution, we integrate both $\eta(z)$ and $\eta_0(z)$ for a range of SN rate models, $r(z) \propto (1+z)^\nu$, over the redshift bins shown in Figure 1. The resulting bias, defined as $\Delta N/N = (N - N_0)/N$, where N is the number of observed SNe and N_0 is the number of underlying SNe in each bin, is at the few percent

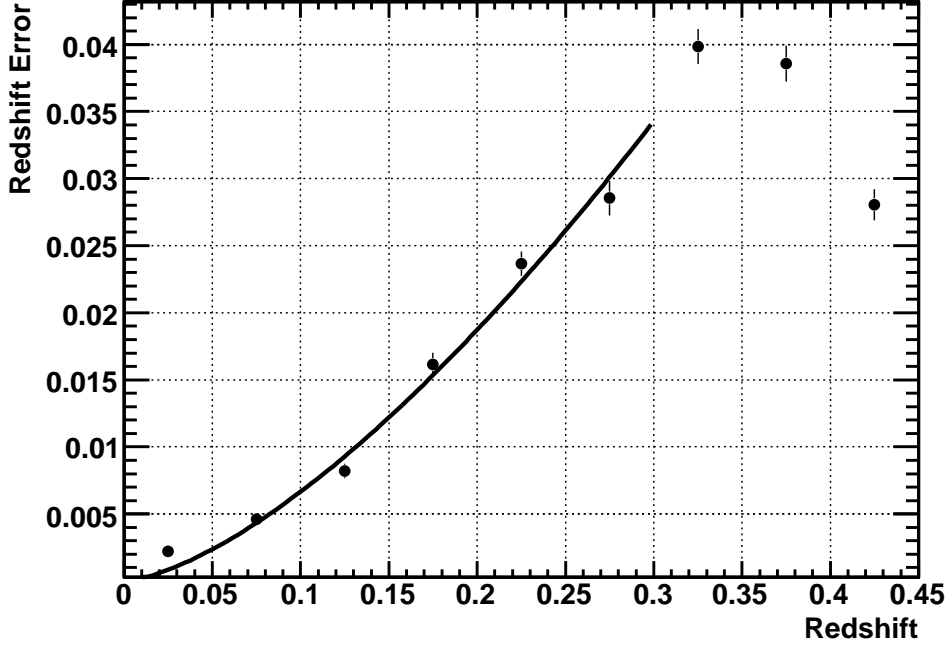


Fig. 3.— The standard deviation of the SN photo- z estimates as a function of fitted photo- z . The points show the mean value of the photo- z error, in bins of width $\delta z = 0.05$. The error bars represent the uncertainty in the mean, and the solid line represents the best-fit power law for the interval $0 < z < 0.3$.

level and is shown in Figure 4. We note that we have considered here a hypothetical SN sample where all the redshifts are determined photometrically. The bias in the observed SDSS-II Supernova Survey SN distribution will be much smaller, since many of the redshifts are determined spectroscopically. In Table 5 we list the bias correction appropriate for our best-fit power-law SN rate model, $r_V(z) \propto (1+z)^{2.04}$, computed over bins in redshift of width $\delta z = 0.05$. The bias due to the use of SN photometric redshifts is negligible in comparison to the statistical and systematic uncertainties on the SN Ia rate measurements. Additionally, we note that in §5.2 we fit the SDSS-II Supernova Survey data to models of the SN rate using an unbinned maximum likelihood that properly accounts for the bias discussed here.

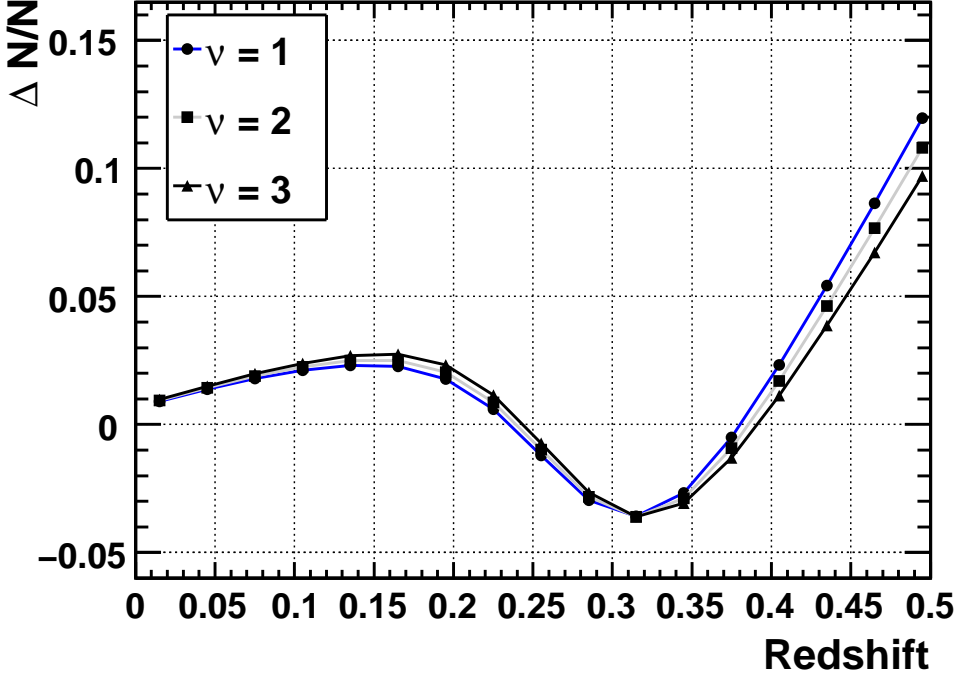


Fig. 4.— The bias, $\Delta N/N$, in an observed distribution of SNe, with a typical error in the measured redshifts (§3.3) and discovery efficiency (§3.1) as determined for the SDSS-II Supernova Survey. The bias is plotted for a range of power-law SN rate models, $r(z) = A_p(1+z)^\nu$.

3.4. Estimating Contamination from Non-Ia SNe

In studies of SNe Ia that include photometrically identified SNe, one must correct for contamination from non-Ia (mainly core-collapse) SNe and evaluate the corresponding systematic uncertainty. Non-Ia SNe form a less homogeneous set than Type Ia SNe and, in contrast to SNe Ia, no general parametric models exist to describe the light curves of non-Ia SNe. In addition, owing to the strong interest in the use of SNe Ia as cosmological distance indicators, there is often an explicit observational bias *against* spectroscopic follow-up observations of non-Ia SNe in modern SN surveys (e.g., Sullivan et al. 2006a; Sako et al. 2008). As the global set of well-observed SNe Ia has grown, this limitation for future SN Ia studies has been recognized, and non-Ia SN observations, in part to better characterize the underlying SN population, are gaining increased attention (e.g., Gal-Yam et al. 2005, 2007).

For these reasons, it is difficult to quantify contamination of the set of photometric

SN Ia candidates from non-Ia SNe in the same way that we have treated determination of the completeness of the SN Ia sample — namely, by modeling the SN survey observations of the underlying population with our SN Monte Carlo simulations. To place limits on the expected level of contamination of the photometric SN sample by non-Ia SNe, we instead consider the set of spectroscopically confirmed non-Ia SNe from the SDSS-II Supernova Survey. There are 42 spectroscopically confirmed non-Ia SNe from the first two years of the SDSS-II Supernova Survey, and an additional 45 from the third year. The reason for the greater relative number of non-Ia SNe in the third year is that, in addition to the usual SN Ia search, the third season included spectroscopic observing time on the Subaru telescope specifically allocated for Type II SNe (D’Andrea et al. 2010). The redshift distribution for the spectroscopically confirmed non-Ia SNe from all three years of the SDSS-II Supernova Survey is shown in Figure 5.

To investigate possible contamination from non-Ia SNe, we apply to the set of non-Ia SNe the same light-curve fits (to a SN Ia model) and selection criteria that are used in defining the SN Ia sample. As the set of photometric SN Ia candidates includes SNe both with and without spectroscopically measured redshifts, we consider contamination from both distance and photo- z fits for the confirmed non-Ia SN sample. If we fix the redshift to its spectroscopically determined value and fit the set of non-Ia SNe for distance, two events satisfy the selection criteria for the SN Ia rate sample. These are SDSS-SN 14492 (SN 2006jo), a SN Ib at $z = 0.077$, and SDSS-SN 17422 (no IAU designation), a SN II at $z = 0.149$. The light-curve fits using the MLCS2k2 SN Ia model for these SNe are shown in Figure 6. If we instead fit the set of non-Ia SNe for photo- z , three of them satisfy the selection criteria for the SN Ia rate sample. These include the two non-Ia SNe mentioned above, as well as SDSS-SN 8679 (SN 2005jr), a SN IIn at $z = 0.294$. If we assume that the fraction of non-Ia SNe that satisfy the selection criteria, q_{CC} , is a random variable that follows a binomial distribution, then an observation of two successful events out of 87 in total gives 1σ limits on q_{CC} of $0.023^{+0.030}_{-0.015}$. An observation of three successful events gives 1σ limits on q_{CC} of $0.035^{+0.032}_{-0.019}$.

Some care must be taken when interpreting the fits to the spectroscopically confirmed non-Ia SNe as an estimate of the false-positive rate. The spectroscopic incompleteness of the SDSS-II Supernova Survey for non-Ia SNe is not well constrained, and the set of spectroscopically confirmed non-Ia SNe is manifestly *not* complete. As mentioned above, the distribution of non-Ia SN light-curve properties is not well measured, so it is difficult to evaluate whether these non-Ia SNe are a representative sampling of the underlying population. However, as the SDSS-II Supernova Survey has a built-in selection bias *against* non-Ia SNe (Sako et al. 2008), it can plausibly be claimed that any bias in the SDSS-II Supernova Survey non-Ia sample is a bias *toward* the most “SN Ia-like” non-Ia SNe. With that being

the case, our estimate of $\sim 3\%$ probability for non-Ia SNe to satisfy our selection criteria can be considered a conservative upper bound.

To turn this into an estimate of the contamination of the photometric SN sample from non-Ia SNe, we must also make an estimate of the non-Ia SN rate. In the redshift range containing the majority of photometric SNe from the SDSS-II Supernova Survey, $0.2 < z < 0.3$, the ratio of the non-Ia SN rate to the SN Ia rate has been measured by Botticella et al. (2008) as $(r_{\text{CC}}/r_{\text{Ia}})_{z=0.25} = 5.6 \pm 3.5$ and by Bazin et al. (2009) as $(r_{\text{CC}}/r_{\text{Ia}})_{z=0.30} = 4.5 \pm 1.0$. Assuming the ratio is constant for $0.2 < z < 0.3$ and combining the two measurements gives a ratio of the non-Ia SN rate to the SN Ia rate of $r_{\text{CC}}/r_{\text{Ia}} = 4.6 \pm 1.0$.

Furthermore, the above estimate of $\sim 3\%$ of non-Ia SNe satisfying the SN Ia selection criteria was determined for SNe that were detected by the SDSS-II Supernova Survey and some estimate must be made of the detection efficiency. To estimate the ratio of detection efficiency for non-Ia SNe vs. SNe Ia, we employ the following procedure. The efficiency for SNe Ia to satisfy the MLCS2k2 component of the selection function (i.e., the items listed in §3.1) as a function of redshift, shown in Figure 8, is transformed to an efficiency as a function of observer-frame peak magnitude by assuming a typical peak absolute magnitude for SNe Ia of $M_B = -19.3$, and a distance modulus derived from a standard Λ CDM cosmological model. This is a good operational definition for detection, since the primary requirements of the MLCS2k2 selection criteria are requirements on the SN sampling and signal-to-noise ratios. Although non-Ia SNe clearly differ from SNe Ia in properties such as light-curve shapes and K-corrections, we will assume that the detection efficiency for non-Ia SNe can be described by the same function of observer-frame magnitude; the efficiency function can then be mapped back to an efficiency as a function of redshift, given an assumed absolute magnitude.

Richardson et al. (2002, 2006) give estimates of the typical peak absolute magnitude for SNe Ib/c as $M_B = -18.07$, for SNe II-P as $M_B = -16.98$, and for SNe II-L as $M_B = -18.17$. Assuming an absolute magnitude of $M_B \approx -18.0$ for non-Ia SNe, the ratio of detection efficiencies for non-Ia SNe vs. SNe Ia as a function of redshift is then computed, and is well approximated by a function $\epsilon_{\text{CC}}^D/\epsilon_{\text{Ia}}^D = 1/(1 + e^{(z-z_0)/s_z})$. The best-fit parameters are found to be $z_0 = (0.204, 0.213, 0.211)$ and $s_z = (0.032, 0.032, 0.031)$ for the 2005, 2006, and 2007 seasons, respectively. The ratio of non-Ia to Ia SNe in the set of photometric SNe can then be estimated as

$$\frac{N_{\text{CC}}}{N_{\text{Ia}}} = \frac{r_{\text{CC}}}{r_{\text{Ia}}} \frac{\epsilon_{\text{CC}}^q}{\epsilon_{\text{Ia}}^q} \frac{\epsilon_{\text{CC}}^D}{\epsilon_{\text{Ia}}^D}, \quad (5)$$

where r is the SN rate, ϵ^q is the efficiency for a SN to satisfy the selection criteria on light-curve shape and fit probability, and ϵ^D is the efficiency for detection, as described

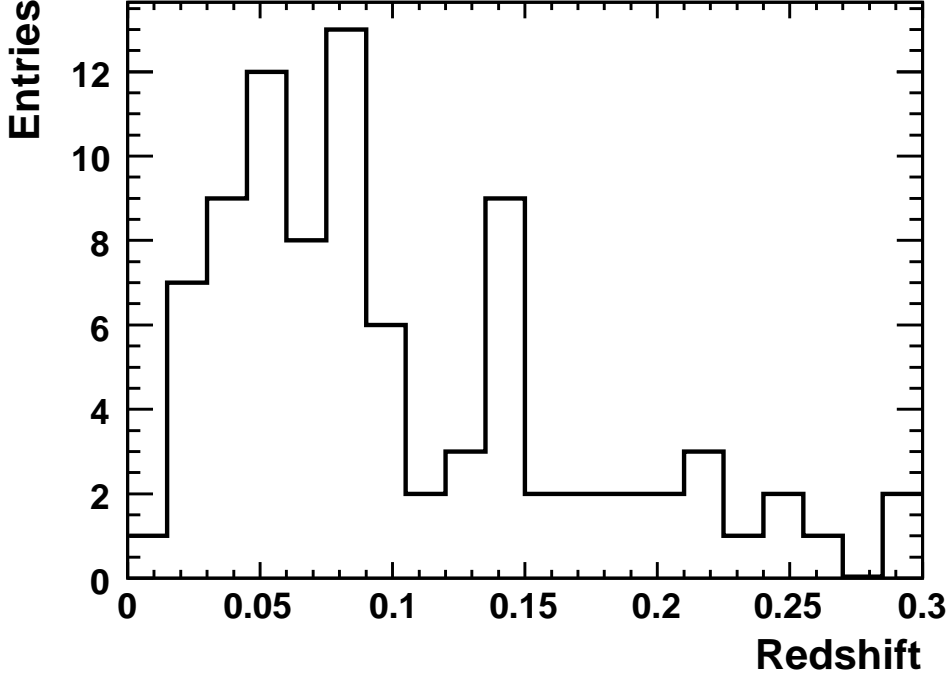


Fig. 5.— Redshift distribution for spectroscopically confirmed non-Ia SNe for the 2005–2007 observing seasons of the SDSS-II Supernova Survey.

above. We note that the ratio of core-collapse SNe to SNe Ia given by Eq. 5 is a function of redshift. For the redshift range of interest, we take $r_{\text{CC}}/r_{\text{Ia}} = 4.6 \pm 1.0$ as discussed above. The quantity $\epsilon_{\text{CC}}^q/\epsilon_{\text{Ia}}^q$ is $0.023^{+0.030}_{-0.015}$ for SNe with spectroscopically measured host-galaxy redshifts and $0.035^{+0.032}_{-0.019}$ for SNe without spectroscopically measured host-galaxy redshifts, as estimated from the spectroscopically confirmed non-Ia SNe in the SDSS-II Supernova Survey.

The estimated core-collapse contamination fraction as a function of redshift is shown in Figure 7, and the corresponding values are given in Table 5. The total estimated contamination of the SN sample by non-Ia SNe to a redshift limit of 0.3 is $2.04^{+1.61}_{-0.95}\%$. In the unbinned maximum-likelihood fits discussed in §5.2, each photometric SN is given a weight according to the value of Eq. 5.

Table 1. Number of SNe Ia for Rate Measurement

Redshift Limit	Confirmed (Spect- z)	Photometric (Spect- z)	Photometric (Photo- z)	Total
0.15	72 (91%)	5 (6%)	2 (3%)	79
0.20	140 (74%)	35 (18%)	15 (8%)	190
0.25	217 (62%)	76 (22%)	57 (16%)	350
0.30	270 (52%)	113 (22%)	133 (26%)	516
∞	312 (40%)	148 (19%)	314 (41%)	774

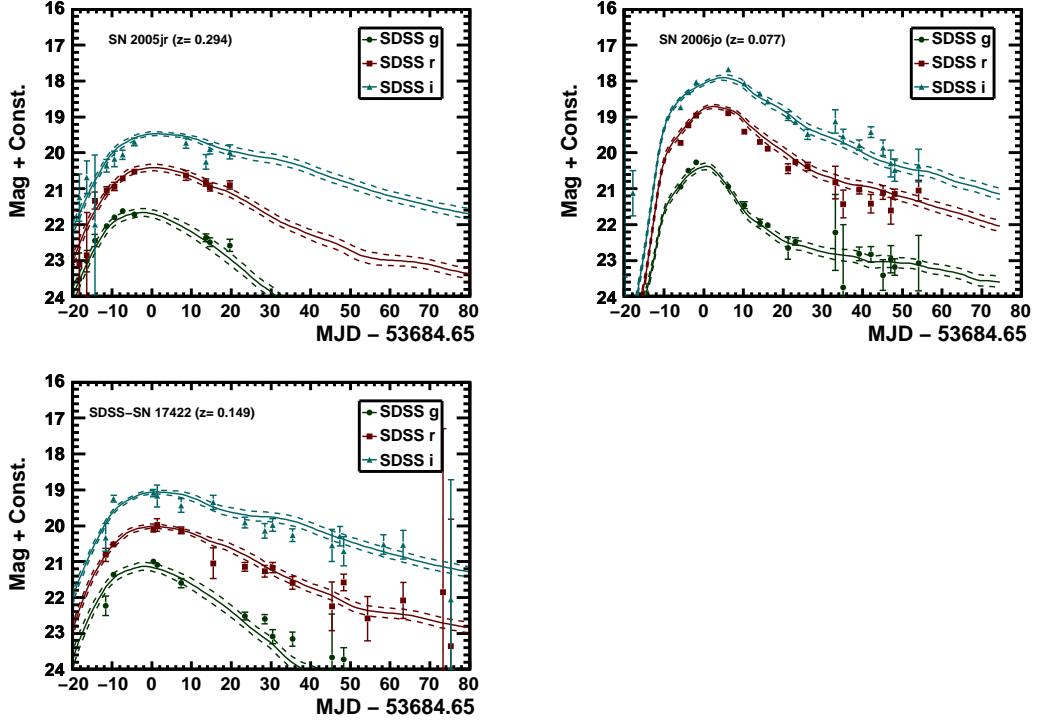


Fig. 6.— Photo- z light-curve fits, to a SN Ia model, for the non-Ia SNe SDSS-SN 8679 (top-left panel), SDSS-SN 14492 (top-right panel), and SDSS-SN 17422 (bottom-right panel). The points represent the observed SN magnitudes, as a function of time, in the observer frame. The solid lines represent the best-fitting model light curves, for the SDSS g , r , and i filter bands, and the dashed lines represent the corresponding 1σ MLCS2k2 model errors. For clarity, the g , r , and i light curves are offset by +0, +1, and +2 mag, respectively.

4. Survey Efficiency

The use of artificial SNe (fakes) in the survey discovery images and the SDSS-SN Monte Carlo (MC) simulation to determine the SN discovery and selection efficiency have been discussed in detail by Dilday et al. (2008). For the MC simulation, for all observing epochs of the SDSS-II Supernova Survey, SN Ia photometry is generated based on a SN Ia light-curve model (MLCS2k2 in the present analysis), and the observing conditions corresponding to each epoch are used to generate realistic photometry errors. Characteristics of the simulated SN sample, such as distributions of time of maximum light, dust extinction, and intrinsic luminosity or decline rate, can be specified in order to simulate a realistic SN sample and to investigate systematic effects of variations in the underlying distributions.

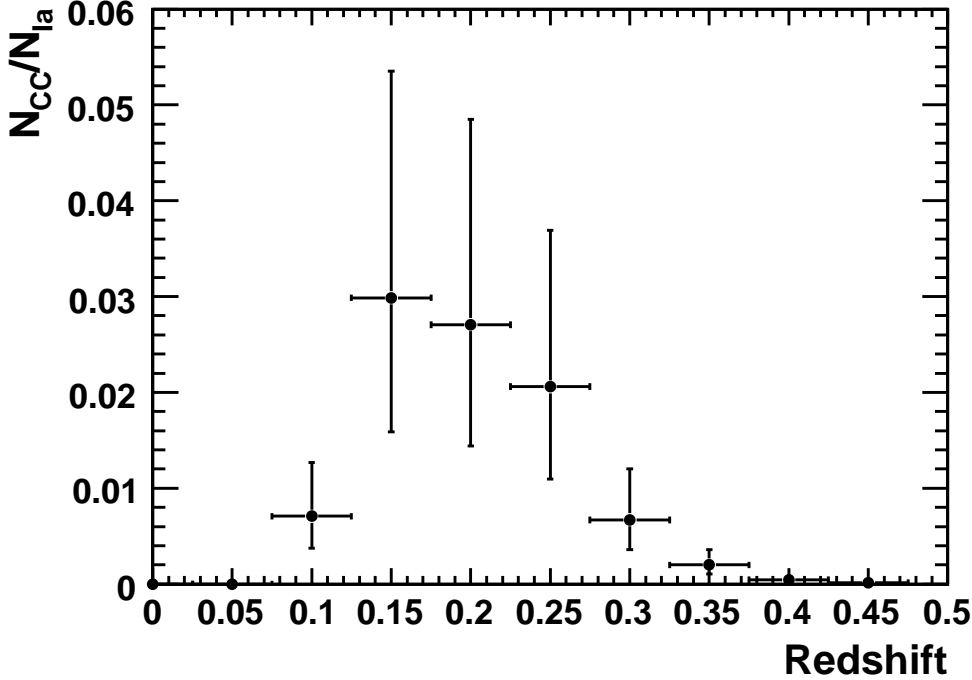


Fig. 7.— Estimated core-collapse contamination fraction vs. redshift.

Here we discuss the effect on the SN discovery efficiency of the modified selection procedure that uses statistics of the photometric-typing fits. To study the SN discovery efficiency for this SN rate analysis, we used the SDSS-SN MC simulation to generate a sample of $\sim 17,000$ MC SNe Ia, which comprises ~ 1000 SNe in each of 17 narrow redshift bins in the range $0.025 < z < 0.4$. These MC SNe were filtered through a simulation of the search detection efficiency. That is, the efficiencies as a function of signal-to-noise ratio determined from the fakes (Dilday et al. 2008) were applied to the simulated MC photometry. As in the search pipeline, a detection in at least two of the *gri* filters is required for the point to be considered to have been detected and to be included in the fit.

The simulated search photometry was then fit with the same photometric-typing code used during the search, and the cuts outlined in §3 were applied. The resulting selection efficiencies are shown in Figure 8.

As discussed by Sako et al. (2008), the photometric typing can be done with or without utilizing forced photometry (performing difference-imaging photometry at known positions of transient objects) and with or without a prior on the SN redshift (from the host-galaxy

photometric or spectroscopic redshift measurement). The selection cuts are applied to fits that *do not* use forced photometry and *do not* use a prior on the SN redshift. While it is evident from examining the photometric-typing fits during the SN search campaign that utilizing forced photometry and/or a prior on the SN redshift in many cases improves the ability to distinguish SNe Ia based on their search-photometry light curves, it is significantly more difficult to model the selection function. The additional complications arise because forced photometry was applied nonuniformly to the SDSS-SN candidates, and because modeling the distribution of host-galaxy photometric redshifts and their errors is nontrivial (Oyaizu et al. 2008).

4.1. Systematic Studies of the SN Discovery Efficiency

In Dilday et al. (2008), we considered the effect on the SN rate discovery efficiency of variation in the distribution of SN population parameters and found that varying the distribution of extinction values had by far the largest effect. Here we repeat the systematic variation of the assumed extinction distribution with the modified selection procedure used in this paper. We vary the input extinction distribution, $p(A_V) \propto e^{-A_V/\tau}$, with $\tau = 0.35 \pm 0.1$. The mean value and variation of A_V are based upon investigation of the underlying A_V distributions presented in the SDSS-SN cosmology analysis (Kessler et al. 2009). We find that for a low-extinction set of SNe ($\tau = 0.25$), the efficiency differs negligibly from the default value of $\tau = 0.35$. However, if the characteristic extinction is large ($\tau = 0.45$), the efficiency differs markedly from the fiducial set of SNe, particularly for $z \gtrsim 0.2$. Comparison of the efficiency between the fiducial and high-extinction assumptions is shown in Figure 8 (right panel). In Table 5 it can be seen that the systematic uncertainty in the SN rate due to uncertainty in the extinction distribution becomes comparable to the statistical uncertainty for $z \approx 0.15$.

5. SN Ia Rate Results

5.1. Constant SN Ia Rate Model

We first consider interpretations of the SN observations described above using a model of the SN rate that is constant as a function of redshift. In a constant-rate model, the volumetric rate is given by

$$r_V = \frac{N}{\widetilde{V}T\epsilon}, \quad (6)$$

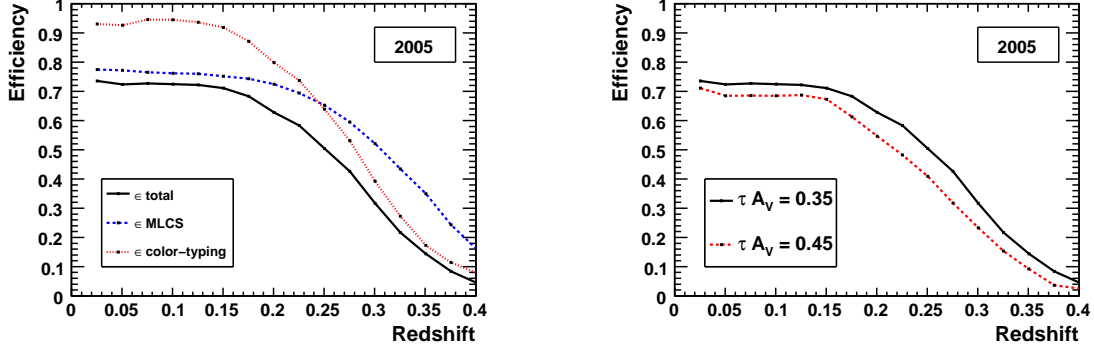


Fig. 8.— Results of studies of the SDSS-SN discovery efficiency, as a function of redshift, based on MC SN samples, for the 2005 observing season. The left panel shows the SN selection efficiency for the photometric-typing (red/dashed), MLCS2k2 (blue/dashed), and combined (black/solid) selection criteria. The right panel shows the efficiency for two different assumptions about the distribution of the extinction parameter, A_V . The A_V distribution is assumed to have the form $e^{-A_V/\tau}$. The efficiency is shown for $\tau = 0.35$ (default) and for $\tau = 0.45$ (1σ upper limit). The values for $\tau = 0.25$ (1σ lower limit) are not shown since they are indistinguishable from the $\tau = 0.35$ values. The efficiency curves for the 2006 and 2007 observing seasons show similar behavior.

where

$$\widetilde{VT\epsilon} = (\Theta T_{\oplus}) \int_{z_{min}}^{z_{max}} \epsilon(z) \frac{d(VT/\Theta)}{dz} dz, \quad (7)$$

N is the number of SNe in the sample, T_{\oplus} is the observation time in the observer frame, Θ is the survey solid angle, $\epsilon(z)$ is the SN discovery efficiency, and $d(VT/\Theta)/dz$ is the element of volume multiplied by time per steradian in the SN frame. In the Friedmann-Robertson-Walker metric, $d(VT/\Theta)/dz$ is given by

$$d(VT/\Theta)/dz = u^2 \frac{du}{dz} \frac{1}{1+z}, \quad (8)$$

$$u(z) = \int_0^z \frac{c}{H(z')} dz'. \quad (9)$$

For the SDSS-II Supernova Survey, the Earth-frame observation time for the 2005–2007 observing seasons are 89, 90, and 90 days, respectively. The solid angle covered is $\Theta = 0.08277 \times 0.98$ steradians. As discussed by Dilday et al. (2008), the regions of the difference

images that corresponded to the locations of bright stars and objects that showed variability in a previous year, and were thus unlikely to be SNe, were excluded (masked) from the search for SNe. This masking accounts for the factor of 98% in the computation of the effective solid angle. The value of the volumetric SN Ia rate, as a function of the upper redshift limit for the SN sample, and derived under the assumption of a constant-rate model, is shown in Figure 9. For example, if the upper redshift limit is chosen as $z = 0.12$, as in Dilday et al. (2008), then the rate is determined to be $r_V = (2.35^{+0.45+0.15}_{-0.39-0.003}) \times 10^{-5}$ SNe yr $^{-1}$ Mpc $^{-3}$ h_{70}^3 (where $h_{70} = H_0/(70 \text{ km s}^{-1} \text{ Mpc}^{-1})$), and the quoted uncertainties are statistical and systematic in that order), based on 37 SNe Ia of which 36 are spectroscopically confirmed. This is lower than, although consistent with, the result found by Dilday et al. (2008), $r_V = (2.93^{+0.90+0.71}_{-0.17-0.04}) \times 10^{-5}$ SNe yr $^{-1}$ Mpc $^{-3}$ h_{70}^3 . In relation to the mean low-redshift SN yield from the three years of the SDSS-II Supernova Survey, the first-year sample presented by Dilday et al. (2008) represented an upward statistical fluctuation. If the upper redshift limit is chosen as $z = 0.15$, where the SN sample still has a high degree of completeness, then the SN Ia rate is determined to be $r_V = (2.69^{+0.34+0.21}_{-0.30-0.01}) \times 10^{-5}$ SNe yr $^{-1}$ Mpc $^{-3}$ h_{70}^3 , based on 79 SNe Ia of which 72 are spectroscopically confirmed.

5.2. SN Ia Rate as a Function of Redshift

In Figure 10, we plot the volumetric SN Ia rate in running bins of width $\Delta z = 0.05$. The rate in each bin is computed by assuming the rate to be constant within the bin, which is a good approximation for the small bins considered. The SN rate values are listed in Table 5. It can be seen that the systematic uncertainty in the selection function (due to uncertainty in the extinction distribution) becomes much larger than the statistical uncertainty for $z \gtrsim 0.2$.

As in Dilday et al. (2008), we employ an unbinned maximum-likelihood method to fit the SN rate data to models of the rate as a function of redshift. To review the method, each SN redshift, z^i , is assumed to be drawn from a probability distribution,

$$p_z^i dz = \langle N \rangle^{-1} \Theta T_{\oplus} \epsilon(z^i) r_V(z^i) d(VT/\Theta)/dz dz, \quad (10)$$

where $r_V(z)$ is the volumetric rate as a function of redshift, $\langle N \rangle$ is the mean number of expected SNe, and the other symbols have been defined in Eq. 7. A likelihood function, L , can then be formed as a product of the individual probabilities, p_z^i , multiplied by a Poisson distribution of the observed number of SNe, N_{SNe} ,

$$L = \frac{\langle N \rangle^{N_{\text{SNe}}} e^{-\langle N \rangle}}{(N_{\text{SNe}})!} \prod_{i=1}^{N_{\text{SNe}}} p_z^i. \quad (11)$$

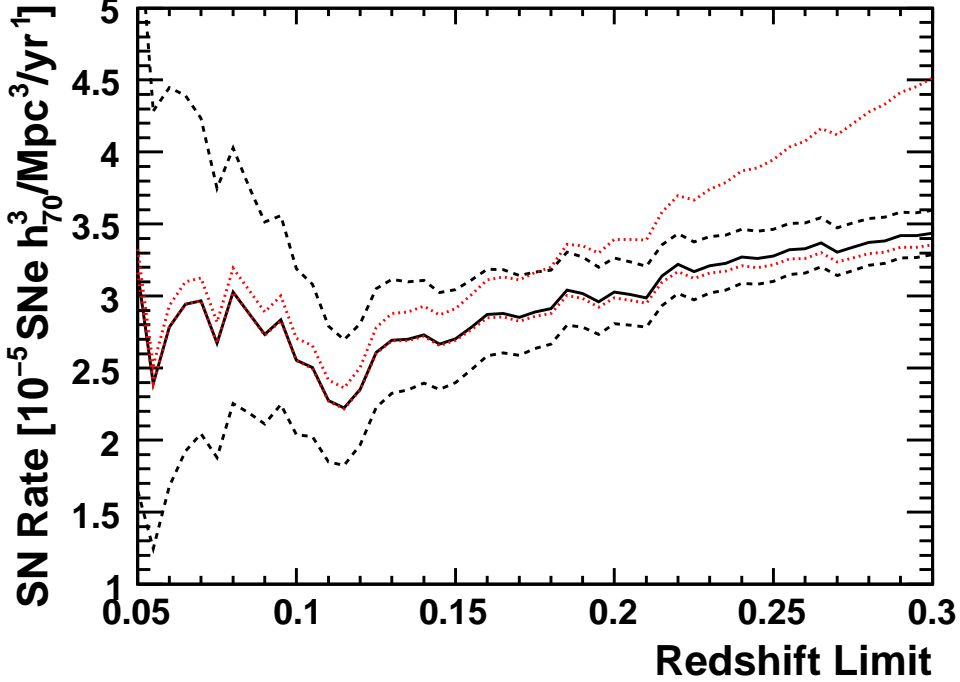


Fig. 9.— The SN Ia rate, assuming a constant-rate model, as a function of upper limit on the redshift range (solid line). The black dashed lines denote the 1σ statistical (Poisson) errors. The red dotted lines show estimates of the systematic errors, which include uncertainty in the SN extinction distribution and estimation of contamination of the SN Ia sample from non-Ia SNe.

When the SN redshifts are determined photometrically, the uncertainties in the measurements are significant, and the individual probabilities must be modified as

$$p_z^i = \langle N \rangle^{-1} \Theta T_{\oplus} \int_{-\infty}^{\infty} \epsilon(z') r_V(z') d(VT/\Theta)/dz' \rho(z'|z^i) dz', \quad (12)$$

where $\rho(z'|z^i)$ is the probability that a SN at redshift z^i will have a measured redshift z' . We assume a Gaussian form for ρ ,

$$\rho(z'|z^i) = \frac{1}{\sqrt{2\pi}\sigma_z} e^{-(z'-z^i)^2/2\sigma_z^2}, \quad (13)$$

where σ_z is the uncertainty in the SN redshift, as determined by the SN photo- z fits. The

parameters of the SN rate model, r_V , are then estimated by minimizing the negative log of the likelihood function. This procedure automatically accounts for the bias in the observed SN redshift distribution described in §3.3. As discussed in §3.4, contamination of the photometric SN sample by non-Ia SNe is accounted for by weighting each photometric SN according to Eq. 5.

Using the maximum-likelihood formalism described above, we consider an empirical power-law model of the SN rate as a function of redshift, $r_V(z) = A_p ((1+z)/(1+z_0))^\nu$. The reference redshift is $z_0 = 0.21$, and the SNe Ia used in the fit are those with $z \leq 0.3$. Our minimization and error analysis are performed with the MINUIT software package, and using the MINOS procedure for asymmetric error estimation (James & Roos 1994). For the power-law rate model, the maximum-likelihood estimates of the model parameters are $A_p = (3.43^{+0.15}_{-0.15}) \times 10^{-5}$ SNe yr⁻¹ Mpc⁻³ h_{70}^3 and $\nu = 2.04^{+0.90}_{-0.89}$, with correlation coefficient $\rho = -0.019$. The uncertainties quoted above are the 1σ statistical errors, defined as the change in the parameter values such that the log-likelihood function changes by 0.5. As discussed in §4.1, uncertainty in the extinction distribution for SNe Ia has a significant impact on the survey efficiency, as inferred from MC simulations, particularly for $z \gtrsim 0.2$ (Fig. 10). Assuming a larger mean value ($\langle A_V \rangle = 0.45$ mag) for the extinction parameter, A_V , and reevaluating the maximum-likelihood estimates for the rate model parameters, results in $A_p = (4.38^{+0.20}_{-0.19}) \times 10^{-5}$ SNe yr⁻¹ Mpc⁻³ h_{70}^3 and $\nu = 4.66^{+0.93}_{-0.92}$, for the parameters of the power-law rate model.

The power-law SN rate models, along with a selection of SN Ia rate measurements from the literature, are shown in Figure 10. SN Ia rate measurements from the SDSS-II Supernova Survey, computed in bins of width $\Delta z = 0.05$ (Table 5), are also shown. We emphasize that the binned SDSS-II Supernova Survey points are shown for convenience and ease of comparison, and that the power-law rate models are derived from the unbinned maximum-likelihood method (§5.2). This plot illustrates the much greater statistical precision of the SDSS-II Supernova Survey in comparison to previous SN Ia rate measurements in the redshift range $0.1 \lesssim z \lesssim 0.3$. Additionally, the SDSS-II Supernova Survey SN Ia rate measurements in the redshift range $0.1 \lesssim z \lesssim 0.2$ have a relatively small systematic uncertainty, and constrain the SN Ia rate to $\sim 10\text{--}20\%$ *total* uncertainty. For $z \gtrsim 0.2$, the systematic uncertainty in the SDSS-II Supernova Survey SN Ia rate measurements becomes much greater than the statistical uncertainty. Despite this large systematic uncertainty, the SDSS-II Supernova Survey SN Ia rate measurements have precision comparable to that of the best existing measurements. Finally, we note that the direction of the systematic uncertainty in the SDSS-II Supernova Survey SN Ia rate measurements is toward an increase in the SN rate. Therefore, the SN Ia rate measurements presented here provide quite robust lower limits on the SN Ia rate at $z \lesssim 0.3$.

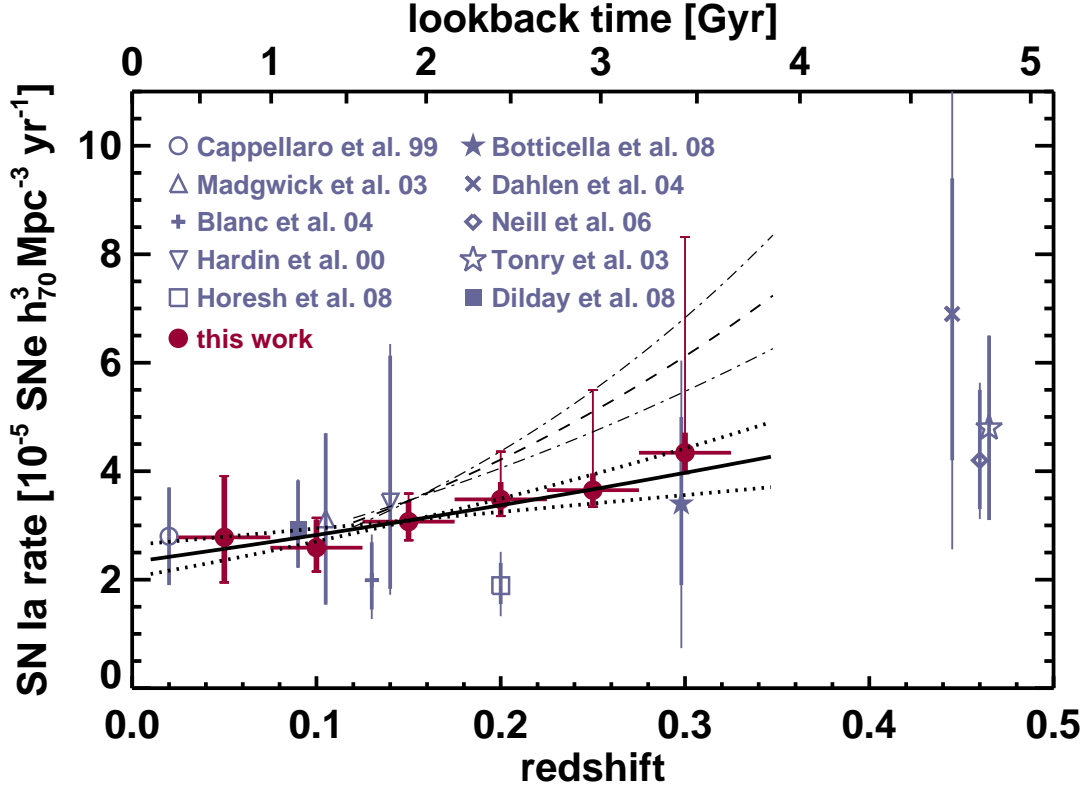


Fig. 10.— SN Ia rate as a function of redshift for the present work, along with a selection of measurements from the literature. For the measurements presented in this work, the redshift is the median redshift of running bins of size $\Delta z = 0.05$, and the SN rate is computed assuming that the rate is constant in each bin. The thick error bars denote the statistical uncertainty while the thin error bars denote the systematic uncertainty. The solid line shows the best-fit power-law rate model, and the dotted lines the 1σ uncertainty of the best-fit model. The dashed line shows the best-fit power-law rate model (plotted only for $z \geq 0.12$), assuming a larger mean value of dust extinction (§4.1), and the dash-dotted line shows the corresponding 1σ uncertainty of the rate model. Some of the SN Ia rate measurements from the literature have been offset in redshift for clarity.

6. Conclusions

We have measured the volumetric SN Ia rate based on the SDSS-II Supernova Survey using a much larger sample of SNe Ia and a higher redshift limit than was discussed by Dilday et al. (2008). The sample of SNe considered comprises 516 SNe Ia at $z \lesssim 0.3$. The low-redshift portion of the SN Ia sample has a high degree of spectroscopic completeness,

while the large redshift range covered enables measurement of the redshift dependence of the SN Ia rate based on the SDSS-II Supernova Survey data alone. Fitting a power-law model to the SN Ia rate, $r_V(z) = A_p ((1+z)/(1+z_0))^\nu$, and assuming a distribution for dust extinction as in Kessler et al. (2009), we find $\nu = 2.04^{+0.90}_{-0.89}$. Assuming a larger mean value of dust extinction we find $\nu = 4.66^{+0.93}_{-0.92}$.

The results presented here represent an order of magnitude improvement in the statistics for SN Ia rate measurements in the same redshift range and solidify the SN Ia rate constraints for $z \lesssim 0.3$. When combined with improved measurements of the cosmic star formation history, the SN Ia rate measurements presented here can be used to place improved constraints on SN Ia progenitor models.

Table 2. Confirmed SNe Ia in the Rate Sample

SN ID	IAU Name	$\alpha_{\text{J}2000}$ [degrees]	$\delta_{\text{J}2000}$ [degrees]	Redshift	Fitprob
762	2005eg	+15.53518	-0.87907	0.191	0.945
1032	2005ez	+46.79565	+1.11952	0.130	0.541
1112	2005fg	-20.98239	-0.37527	0.258	0.792
1166	...	+9.35560	+0.97320	0.382	0.992
1241	2005ff	-22.32751	-0.77664	0.090	0.988
1253	2005fd	-36.20105	+0.16305	0.262	0.834
1371	2005fh	-10.62625	+0.42929	0.119	0.995
1580	2005fb	+45.32296	-0.64412	0.183	1.000
1688	...	-38.64233	+0.32447	0.359	0.183
2017	2005fo	-31.05673	+0.59343	0.262	0.972
2031	2005fm	-47.95688	-1.17149	0.153	0.894
2165	2005fr	+17.09165	-0.09639	0.288	0.930
2246	2005fy	+50.09031	-0.88564	0.195	0.904
2308	2005ey	+34.27273	+0.28020	0.148	0.960
2330	2005fp	+6.80699	+1.12053	0.213	0.841
2372	2005ft	+40.52065	-0.54088	0.181	0.996
2422	2005fi	+1.99444	+0.63811	0.265	0.867
2440	2005fu	+42.63359	+0.80774	0.193	0.859
2533	2005fs	+31.22063	-0.32655	0.340	0.995
2561	2005fv	+46.34335	+0.85829	0.118	1.000

Table 2—Continued

SN ID	IAU Name	α_{J2000} [degrees]	δ_{J2000} [degrees]	Redshift	Fitprob
2635	2005fw	+52.70425	-1.23815	0.144	0.994
2689	2005fa	+24.90027	-0.75879	0.162	0.230
2789	2005fx	-15.79858	+0.40102	0.290	0.231
2916	2005fz	-44.07831	+0.56948	0.124	0.341
2943	2005go	+17.70491	+1.00784	0.265	0.744
2992	2005gp	+55.49692	-0.78269	0.127	0.385
3080	2005ga	+16.93231	-1.03955	0.175	0.999
3087	2005gc	+20.40666	-0.97730	0.166	1.000
3199	2005gs	-26.70743	+1.05048	0.251	0.817
3241	2005gh	-47.34857	-0.35416	0.259	0.219
3331	2005ge	+34.56134	+0.79646	0.213	0.993
3377	2005gr	+54.15606	+1.07909	0.245	0.999
3451	2005gf	-25.93079	+0.70805	0.250	0.814
3452	2005gg	-25.32861	+0.63906	0.230	0.957
3592	2005gb	+19.05240	+0.79183	0.087	1.000
3901	2005ho	+14.85039	+0.00252	0.063	1.000
4046	2005gw	-5.50177	+0.64201	0.277	0.955
4241	2005gu	+12.23758	-0.90583	0.332	0.176
4577	2005gv	+38.47543	+0.28062	0.363	0.994
4679	2005gy	+21.52825	+0.67678	0.332	0.413

Table 2—Continued

SN ID	IAU Name	$\alpha_{\text{J}2000}$ [degrees]	$\delta_{\text{J}2000}$ [degrees]	Redshift	Fitprob
5103	2005gx	-0.11563	+0.73711	0.162	0.993
5350	2005hp	-52.78091	-0.77928	0.175	0.999
5395	2005hr	+49.64084	+0.12327	0.117	1.000
5533	2005hu	-31.33014	+0.41335	0.220	0.733
5549	2005hx	+3.25048	+0.24814	0.121	0.997
5550	2005hy	+3.59819	+0.33297	0.156	0.988
5635	2005hv	-26.81729	-0.03503	0.179	0.943
5717	2005ia	+17.89588	-0.00597	0.252	0.999
5736	2005jz	+22.86264	-0.63166	0.253	0.962
5737	2005ib	+22.85692	-0.60344	0.393	0.890
5751	2005hz	+11.63408	+0.83812	0.131	0.999
5844	2005ic	-32.21384	-0.84302	0.311	0.837
5916	2005is	+5.43728	-0.32510	0.175	0.923
5957	2005ie	+34.76051	-0.27292	0.280	0.840
5994	2005ht	-47.39755	-0.16795	0.187	0.993
6057	2005if	+52.55355	-0.97467	0.067	1.000
6108	2005ih	+1.80657	+0.34890	0.259	0.993
6127	2005iw	-22.67609	-0.09245	0.280	0.696
6137	2005iv	-52.06393	+0.24473	0.300	0.964
6192	2005jy	-11.53506	+1.25689	0.272	0.837

Table 2—Continued

SN ID	IAU Name	$\alpha_{\text{J}2000}$ [degrees]	$\delta_{\text{J}2000}$ [degrees]	Redshift	Fitprob
6196	2005ig	-22.36893	-0.50279	0.281	0.290
6249	2005ii	+3.26547	-0.62019	0.294	0.897
6295	2005js	+23.67295	-0.60544	0.080	0.005
6304	2005jk	+26.49760	+1.19589	0.191	0.896
6315	2005ix	-49.51727	+1.09191	0.267	0.828
6406	2005ij	+46.08860	-1.06301	0.125	1.000
6422	2005id	-10.86130	-0.66326	0.184	0.954
6558	2005hj	+21.70165	-1.23814	0.057	0.998
6649	2005jd	+34.27582	+0.53471	0.314	0.949
6699	2005ik	-37.18509	-1.05707	0.311	0.894
6773	2005iu	-54.93497	+0.21731	0.090	0.009
6780	2005iz	-31.93149	+0.26698	0.202	0.988
6933	2005jc	+11.35168	+1.07547	0.213	0.951
6936	2005jl	-36.76620	-0.69986	0.181	0.772
7143	2005jg	-14.73767	-0.20746	0.304	0.981
7147	2005jh	-9.98169	-0.05557	0.111	0.080
7243	2005jm	-31.92096	+0.47186	0.204	0.945
7335	2005kn	-41.11487	-0.35543	0.198	0.850
7473	2005ji	+4.32628	-0.25736	0.216	0.942
7475	2005jn	+4.75338	-0.28156	0.322	0.911

Table 2—Continued

SN ID	IAU Name	$\alpha_{\text{J}2000}$ [degrees]	$\delta_{\text{J}2000}$ [degrees]	Redshift	Fitprob
7512	2005jo	+52.09022	-0.32617	0.219	0.708
7779	2005jw	-49.91983	-0.00723	0.381	0.406
7847	2005jp	+32.45985	-0.06185	0.212	0.838
7876	2005ir	+19.18237	+0.79452	0.076	0.298
7947	2005jj	-45.81400	+0.40829	0.368	0.563
8030	2005jv	+40.20864	+0.99305	0.422	0.997
8046	2005ju	+39.11671	+0.51118	0.259	0.998
8213	2005ko	-2.47919	-0.92148	0.185	0.839
8495	2005mi	-24.73898	-0.74820	0.214	0.268
8598	2005jt	+42.66724	-0.06600	0.361	0.991
8707	2005mh	+41.23612	+0.20358	0.395	0.877
8719	2005kp	+7.72141	-0.71893	0.118	0.298
9032	2005le	-22.11548	-0.49365	0.254	0.991
9045	2005kq	-12.16296	-0.60869	0.389	0.788
9467	2005lh	-31.04868	+1.18071	0.218	0.413
10550	2005lf	-10.32468	-1.20496	0.300	0.916
12780	2006eq	-37.84546	+1.22804	0.049	0.997
12853	2006ey	-43.23453	+0.72302	0.169	0.688
12855	2006fk	-29.74451	+0.71614	0.172	0.006
12856	2006fl	-27.13458	+0.75589	0.172	0.990

Table 2—Continued

SN ID	IAU Name	$\alpha_{\text{J}2000}$ [degrees]	$\delta_{\text{J}2000}$ [degrees]	Redshift	Fitprob
12860	2006fc	-36.30588	+1.17579	0.122	0.999
12874	2006fb	-6.03552	-0.17724	0.245	0.795
12898	2006fw	+26.79302	-0.14708	0.083	0.997
12930	2006ex	-50.31729	-0.47460	0.147	0.999
12950	2006fy	-8.33258	-0.84032	0.083	0.987
12972	2006ft	+7.95851	-0.38302	0.261	0.993
12977	2006gh	+13.69553	-0.25095	0.248	1.000
13025	2006fx	-18.43280	+0.41579	0.224	0.925
13038	2006gn	-12.17328	+0.50451	0.104	0.997
13044	2006fm	-27.45731	+0.50323	0.126	1.000
13070	2006fu	-2.21500	-0.74645	0.199	0.820
13072	2006fi	-25.04071	+0.02439	0.231	0.817
13135	2006fz	+4.17214	-0.42463	0.105	0.756
13136	2006go	+6.14062	-0.27912	0.372	0.174
13152	2006gg	+7.05201	+0.11793	0.203	0.935
13174	2006ga	+13.23463	+0.44774	0.236	0.570
13305	2006he	-28.89957	+0.69111	0.214	0.392
14782	2006jp	-45.76578	-0.27913	0.160	0.048
13354	2006hr	+27.56474	-0.88735	0.158	0.681
13411	...	-44.81009	+0.19162	0.163	0.967

Table 2—Continued

SN ID	IAU Name	$\alpha_{\text{J}2000}$ [degrees]	$\delta_{\text{J}2000}$ [degrees]	Redshift	Fitprob
13506	2006hg	+25.24323	-0.72791	0.245	0.013
13511	2006hh	+40.61224	-0.79419	0.238	0.176
13578	2006hc	+17.39463	+0.70404	0.229	0.713
13641	2006hf	-14.78134	-0.98122	0.219	0.393
14157	2006kj	+51.13660	+1.02230	0.212	0.023
13689	...	+4.01602	+0.80747	0.252	0.826
13727	2006hj	-42.41196	+0.93256	0.226	0.451
13736	2006hv	-23.16675	+1.03089	0.150	0.999
13757	2006hk	-9.87695	-1.15792	0.289	0.641
13796	2006hl	-9.30850	+0.53280	0.148	1.000
13835	2006hp	+6.05959	-0.24832	0.248	0.915
13894	2006jh	+1.69050	-0.03686	0.125	0.999
13934	2006jg	-17.88916	-0.43543	0.330	0.437
13956	2006hi	+20.94173	+0.81663	0.262	0.020
14019	2006ki	-43.35767	-0.64799	0.216	0.563
14024	2006ht	-41.80148	+0.91627	0.146	0.707
14108	2006hu	+53.59454	-1.12330	0.133	0.827
14212	2006iy	-29.52997	+1.04491	0.205	0.745
14261	2006jk	-31.75970	+0.25372	0.286	0.963
14279	2006hx	+18.48869	+0.37156	0.045	0.395

Table 2—Continued

SN ID	IAU Name	$\alpha_{\text{J}2000}$ [degrees]	$\delta_{\text{J}2000}$ [degrees]	Redshift	Fitprob
14284	2006ib	+49.04921	-0.60105	0.181	0.237
14298	2006jj	-45.10498	+1.22317	0.270	0.935
14331	2006kl	+7.88862	-0.13590	0.221	0.619
14377	2006hw	+48.26427	-0.47171	0.139	0.744
14421	2006ia	+31.82975	+1.25197	0.175	0.005
14437	2006hy	-27.91913	-1.19642	0.149	0.803
14481	2006lj	+2.68159	+0.20113	0.244	0.482
14735	2006km	+35.15793	+0.34831	0.301	0.858
14816	2006ja	-23.28375	+0.50600	0.107	0.020
14846	2006jn	+7.66319	+0.14148	0.225	0.991
14871	2006jq	+54.27705	+0.00928	0.128	0.997
14979	2006jr	+54.94641	+0.99273	0.177	0.981
14984	2006js	-46.16650	-0.09283	0.197	0.619
15002	2006ko	+22.24966	+0.76984	0.356	0.725
15057	2006md	+17.88118	+0.40941	0.299	0.105
15171	2006kb	-55.20749	-1.06454	0.134	0.995
15129	2006kq	-41.09772	-0.32151	0.199	0.025
15132	2006jt	-30.29984	+0.19764	0.144	0.853
15136	2006ju	-8.83755	-0.71842	0.149	0.023
15161	2006jw	+35.84275	+0.81893	0.250	0.212

Table 2—Continued

SN ID	IAU Name	$\alpha_{\text{J}2000}$ [degrees]	$\delta_{\text{J}2000}$ [degrees]	Redshift	Fitprob
15201	2006ks	-22.48059	+0.00359	0.208	0.352
15203	2006jy	+15.73466	+0.18302	0.204	0.989
15213	2006lk	+53.01909	-0.10022	0.311	0.982
15219	2006ka	+34.61100	+0.22658	0.248	0.879
15222	2006jz	+2.85320	+0.70267	0.199	0.995
15229	2006kr	+4.83195	+1.09059	0.227	0.844
15234	2006kd	+16.95826	+0.82809	0.136	0.978
15254	2006oy	-46.50714	-0.36011	0.201	0.186
15259	2006kc	-22.45593	-0.40788	0.210	0.725
15287	2006kt	-36.04034	-1.05750	0.274	0.909
15301	2006lo	-36.42014	+0.58907	0.296	0.738
15354	2006lp	+6.77357	-0.12606	0.222	0.199
15356	2006lm	-24.94675	+0.40984	0.275	0.162
15365	2006ku	-5.44342	+1.24900	0.188	0.963
15369	2006ln	-11.16714	-0.56267	0.232	0.881
15421	2006kw	+33.74157	+0.60240	0.185	0.981
15425	2006kx	+55.56103	+0.47820	0.160	0.640
15433	2006mt	+14.87962	-0.25662	0.221	0.879
15440	2006lr	+39.72062	+0.09002	0.262	0.801
15443	2006lb	+49.86736	-0.31813	0.182	0.617

Table 2—Continued

SN ID	IAU Name	$\alpha_{\text{J}2000}$ [degrees]	$\delta_{\text{J}2000}$ [degrees]	Redshift	Fitprob
15453	2006ky	-40.33179	-1.02438	0.184	0.999
15456	2006ll	-28.13284	-0.90348	0.382	0.626
15459	2006la	-19.29861	-0.90184	0.127	0.832
15461	2006kz	-33.15259	-0.49477	0.180	0.931
15466	2006mz	-42.35504	-0.12329	0.246	0.930
15467	...	-39.98016	-0.17753	0.210	0.984
15508	2006ls	+27.16886	-0.57666	0.147	0.997
15583	2006mv	+37.73095	+0.94621	0.175	0.911
15584	2006nt	+43.49536	+0.98691	0.282	0.994
15648	2006ni	-46.28171	-0.19488	0.175	0.316
15674	2006nu	-19.17090	+0.26279	0.197	0.796
15776	2006na	+32.82938	-0.99828	0.305	0.046
15704	2006nh	+40.21070	+0.65870	0.365	0.906
15868	2006pa	+38.09978	-0.71369	0.242	0.923
15872	2006nb	+36.72244	-0.32791	0.185	0.941
15897	2006pb	+11.68145	-1.03294	0.175	0.051
15901	2006od	+31.97622	-0.53548	0.205	0.413
16000	2006nj	+21.11753	+0.07430	0.390	0.964
16021	2006nc	+13.84359	-0.38889	0.124	0.457
16032	2006nk	+44.06910	-0.41082	0.204	0.735

Table 2—Continued

SN ID	IAU Name	$\alpha_{\text{J}2000}$ [degrees]	$\delta_{\text{J}2000}$ [degrees]	Redshift	Fitprob
16072	2006nv	+3.12437	-0.97737	0.287	0.896
16073	2006of	+8.10770	-1.05408	0.153	0.955
16093	2006oe	-9.63757	+1.13236	0.335	0.994
16100	2006nl	+30.43619	-1.03248	0.195	0.559
16185	2006ok	+16.86800	-0.26945	0.097	0.987
16211	2006nm	-11.83603	+0.26679	0.311	0.928
17168	2007ik	-20.27621	-1.16716	0.184	0.995
17186	2007hx	+31.61272	-0.89963	0.080	0.989
17332	2007jk	+43.77335	-0.14750	0.183	0.434
17340	2007kl	+41.21201	+0.36474	0.257	0.945
17366	2007hz	-44.21277	-1.02926	0.139	0.993
17389	2007ih	-36.70523	-0.96028	0.171	0.674
17435	2007ka	+20.34463	-0.01488	0.218	0.310
17497	2007jt	+37.13649	-1.04221	0.145	0.991
17552	2007jl	-37.67953	-1.00328	0.254	0.847
17568	2007kb	-46.89713	+0.27759	0.145	0.999
17629	2007jw	+30.63637	-1.08924	0.137	0.324
17745	2007ju	+2.96016	-0.33928	0.064	1.000
17784	2007jg	+52.46166	+0.05676	0.037	1.000
17791	2007kp	-27.62686	+0.73781	0.286	0.526

Table 2—Continued

SN ID	IAU Name	α_{J2000} [degrees]	δ_{J2000} [degrees]	Redshift	Fitprob
17801	2007ko	-43.90686	-0.89806	0.206	0.572
17809	2007kr	+6.36447	-0.83962	0.282	0.934
17811	2007ix	+12.87864	-0.94747	0.213	0.877
17825	2007je	+32.94703	-0.91251	0.161	1.000
17875	2007jz	+20.98331	+1.25488	0.232	0.423
17880	2007jd	+44.97227	+1.16063	0.073	0.934
17884	2007kt	+27.59980	+1.17200	0.239	0.717
17886	2007jh	+54.00627	+1.10330	0.041	0.940
18030	2007kq	+4.93285	-0.40022	0.156	0.170
18091	2007ku	+23.36750	+0.52460	0.372	0.300
18241	2007ks	-47.61234	-0.76182	0.095	0.992
18298	2007li	+18.26664	-0.54014	0.120	0.416
18323	2007kx	+3.42863	+0.65206	0.155	0.893
18325	2007mv	+8.90570	+0.36997	0.255	0.372
18375	2007lg	+11.51640	-0.01046	0.110	0.784
18415	2007la	-22.52173	+1.05851	0.131	0.993
18451	2007mt	+26.48567	-0.21765	0.408	0.711
18456	2007lk	+29.45877	-0.39821	0.219	0.102
18463	2007kv	+17.56589	+0.47195	0.268	0.997
18466	2007lm	+48.41846	+0.62995	0.213	0.988

Table 2—Continued

SN ID	IAU Name	$\alpha_{\text{J}2000}$ [degrees]	$\delta_{\text{J}2000}$ [degrees]	Redshift	Fitprob
18485	2007nu	+47.95904	-0.69255	0.282	0.884
18486	2007ln	+55.17992	+1.00300	0.240	0.994
18602	2007lo	-21.01651	+0.60916	0.138	0.655
18604	2007lp	-19.07919	+0.42131	0.176	0.925
18612	2007lc	+12.28788	+0.59688	0.115	0.796
18650	2007lt	-31.55280	+0.01500	0.113	1.000
18721	2007mu	+3.07724	-0.07738	0.403	0.948
18740	2007mc	+16.85519	+1.04368	0.157	0.995
18749	2007mb	+12.54733	+0.67532	0.189	0.754
18768	2007lh	+17.21666	+1.19777	0.198	0.550
18787	2007mf	+29.72962	-1.02722	0.207	0.998
18804	2007me	+25.26560	-0.44851	0.205	0.941
18807	2007mg	+46.64086	+0.79320	0.158	1.000
18835	2007mj	+53.68503	+0.35546	0.123	1.000
18855	2007mh	+48.63231	+0.26975	0.128	1.000
18890	2007mm	+16.44440	-0.75890	0.066	0.970
18903	2007lr	+12.25138	-0.32410	0.156	0.991
18909	2007lq	+5.78274	+0.98334	0.228	0.816
18927	2007nt	+46.68240	-0.75412	0.213	0.696
18940	2007sb	+10.34886	+0.41188	0.212	0.424

Table 2—Continued

SN ID	IAU Name	$\alpha_{\text{J}2000}$ [degrees]	$\delta_{\text{J}2000}$ [degrees]	Redshift	Fitprob
18945	2007nd	+10.07834	-1.03742	0.263	0.839
18965	2007ne	+13.50917	+1.06891	0.207	0.754
19002	2007nh	+42.61525	-0.55126	0.263	0.999
19008	2007mz	-28.03674	-1.07002	0.232	0.940
19027	2007my	-31.11588	-0.37204	0.293	0.325
19051	2007nb	-8.62479	+0.42302	0.277	0.053
19067	2007oq	-34.37195	+0.98454	0.339	0.494
19101	2007ml	+7.97267	+0.13823	0.187	0.836
19128	2007lw	-5.79630	-0.78234	0.287	0.930
19149	2007ni	+31.45990	-0.33195	0.196	0.670
19155	2007mn	+31.26644	+0.17447	0.077	0.228
19220	2007ox	-18.25815	-0.07193	0.212	0.968
19230	2007mo	-27.10907	+0.76465	0.221	0.463
19282	2007mk	-0.92789	-0.50594	0.186	0.827
19341	2007nf	+15.86018	+0.33129	0.228	0.449
19353	2007nj	+43.11432	+0.25177	0.154	0.888
19543	2007oj	-2.09171	+0.27972	0.123	0.483
19596	2007po	+53.88425	+0.70331	0.292	0.996
19604	2007oi	+5.32441	+1.07446	0.296	0.097
19616	2007ok	+37.10098	+0.18458	0.166	0.963

Table 2—Continued

SN ID	IAU Name	$\alpha_{\text{J}2000}$ [degrees]	$\delta_{\text{J}2000}$ [degrees]	Redshift	Fitprob
19625	2007pn	+34.14118	-0.72247	0.307	0.534
19632	2007ov	+40.28636	+0.14436	0.315	0.951
19658	2007ot	+8.90311	-0.23275	0.200	0.993
19702	2007pp	+47.75470	+0.35671	0.262	0.822
19775	2007pc	-41.04401	+0.65120	0.138	0.936
19794	2007oz	-0.68103	+0.24923	0.297	0.517
19818	2007pe	+35.26666	+0.49634	0.304	0.779
19913	2007qf	-26.23758	-0.34134	0.204	0.212
19940	2007pa	-44.60651	-0.26855	0.157	0.991
19968	2007ol	+24.34869	-0.31209	0.056	0.904
19969	2007pt	+31.91040	-0.32408	0.175	0.972
19990	2007ps	+34.80625	-0.38490	0.246	0.833
19992	2007pb	-2.89594	-1.18509	0.228	0.938
20039	2007qh	+9.87848	+1.02425	0.248	0.899
20040	2007rf	-31.12057	+0.81499	0.288	0.655
20048	2007pq	-20.69196	+0.73627	0.185	0.804
20064	2007om	-1.41388	-0.91773	0.105	0.981
20084	2007pd	-12.02487	-0.57817	0.091	0.686
20088	...	+13.20511	+0.63137	0.244	0.466
20097	2007rd	-48.24554	-0.09939	0.221	0.992

Table 2—Continued

SN ID	IAU Name	α_{J2000} [degrees]	δ_{J2000} [degrees]	Redshift	Fitprob
20106	2007pr	-13.44586	+0.32884	0.333	0.922
20111	2007pw	-5.60574	+0.24802	0.245	0.396
20142	2007qg	+23.00817	-0.42981	0.314	0.997
20184	2007qn	-0.21152	+1.15823	0.324	0.824
20186	2007pj	-2.70554	+0.79778	0.354	0.927
20245	2007pi	-18.29459	+0.75618	0.288	0.976
20345	2007qp	+10.70167	+0.37962	0.265	0.316
20350	2007ph	-47.19424	-0.95590	0.130	0.082
20364	2007qo	+25.75656	-0.94553	0.218	0.671
20376	2007re	-40.60461	-0.52406	0.211	0.001
20768	2007qq	+40.62584	-0.97121	0.238	0.147
20821	2007rk	+55.57257	+1.06302	0.196	0.125

Table 3. SNe with Spectroscopic Redshifts in the Rate Sample

SN ID	$\alpha_{\text{J}2000}$ [degrees]	$\delta_{\text{J}2000}$ [degrees]	Redshift	Fitprob
703	-23.78214	+0.65059	0.300	0.976
779	+26.67369	-1.02072	0.238	0.986
911	+38.69067	-0.11571	0.208	0.930
1008	+28.27810	+1.11369	0.226	0.974
1415	+6.10647	+0.59921	0.212	0.924
1740	+5.40428	-0.88099	0.167	0.013
2057	-39.60031	-0.31708	0.212	0.512
2081	-22.69495	-1.20783	0.252	0.753
2162	+15.44242	-0.13368	0.173	0.777
2532	+27.74742	-0.23427	0.270	0.913
2632	+45.59013	-1.22610	0.296	0.044
2639	-29.53589	+0.66447	0.215	0.278
2734	+48.20686	-0.69485	0.303	0.149
2806	+45.26690	+0.27364	0.301	0.340
2864	-0.54910	-1.23960	0.244	0.426
3049	-29.77658	-1.23657	0.167	0.936
3195	+8.66830	+0.24421	0.300	0.135
3488	-46.44482	-1.01043	0.160	0.003
3535	+44.11722	-0.13357	0.308	0.952
3881	-8.11838	-0.44181	0.328	0.438

Table 3—Continued

SN ID	$\alpha_{\text{J}2000}$ [degrees]	$\delta_{\text{J}2000}$ [degrees]	Redshift	Fitprob
4019	+1.26167	+1.14534	0.181	0.921
4035	+21.46727	+1.04749	0.428	0.084
4059	+54.64996	+0.14576	0.304	0.107
4181	+37.81778	-1.13101	0.289	0.610
4236	+1.90560	-1.01839	0.343	0.723
4281	+33.36735	-0.96831	0.213	0.984
4307	+29.96247	+0.94960	0.272	0.987
4311	+32.13080	+1.01988	0.295	0.608
4651	+37.37555	-0.74726	0.152	0.938
4676	+18.82365	+0.78805	0.245	0.258
4690	+32.92946	+0.68817	0.200	0.311
5473	-5.26337	+0.38342	0.280	0.725
5486	-26.75208	-0.41210	0.229	0.965
5673	-6.19876	+0.78419	0.379	0.952
5785	-31.40262	+0.08376	0.148	0.120
5890	-27.48444	+0.60915	0.180	0.966
5959	+38.05976	-0.30821	0.208	0.999
5963	+11.08100	+0.47940	0.236	0.996
5993	+29.68238	+0.04895	0.377	0.793
6275	+34.58972	+0.02990	0.273	0.264

Table 3—Continued

SN ID	$\alpha_{\text{J}2000}$ [degrees]	$\delta_{\text{J}2000}$ [degrees]	Redshift	Fitprob
6431	+7.50847	-0.70385	0.252	0.752
6479	-39.59277	+0.58351	0.234	0.444
6530	+14.32909	+0.02129	0.193	0.592
6614	+26.64692	+0.86672	0.169	0.028
6714	-2.64008	+0.63176	0.414	0.523
6851	+52.10445	-0.04860	0.305	0.983
6861	-10.56781	-1.11353	0.190	0.621
6895	-29.80710	+0.92818	0.217	0.799
6903	-24.55649	+0.97167	0.253	0.757
7092	-43.71957	+1.22042	0.225	0.991
7099	-17.11191	+1.16725	0.218	0.950
7102	-35.38019	-0.61565	0.196	0.185
7258	-38.77008	-0.99907	0.255	0.960
7373	-7.19519	+0.58823	0.280	0.886
7431	-19.04562	-0.27500	0.350	0.856
7444	+27.70291	+0.42972	0.250	0.874
7457	-9.09689	-0.37225	0.254	0.072
7527	-24.74368	-1.20414	0.237	0.937
7644	-6.06500	+0.86820	0.310	0.592
7647	-1.61700	+1.04199	0.385	0.718

Table 3—Continued

SN ID	$\alpha_{\text{J}2000}$ [degrees]	$\delta_{\text{J}2000}$ [degrees]	Redshift	Fitprob
7701	+6.51694	-1.22886	0.361	0.864
7824	-11.18698	-0.08091	0.287	0.777
7954	-27.32306	+0.34771	0.255	0.772
8114	-7.78342	+0.22833	0.372	0.704
8165	+50.22528	-1.10940	0.319	0.624
8195	-28.99365	-0.89569	0.269	0.999
8254	-8.83624	+0.81979	0.189	0.067
8280	+8.57363	+0.79595	0.185	0.897
8555	+2.91543	-0.41497	0.198	0.649
8607	-36.41309	+0.15191	0.260	0.491
8742	+11.23943	+0.43712	0.214	0.787
9117	+46.90165	+0.98827	0.272	0.995
9155	-32.64563	-0.78476	0.305	0.974
9594	+17.71423	+0.12161	0.298	0.132
9739	-36.30621	-0.87893	0.120	0.421
11306	+56.73846	-0.51832	0.274	0.994
12804	+18.20149	+1.04017	0.134	0.995
12852	-45.74695	+0.68913	0.264	0.501
15386	-47.41525	-1.23257	0.287	0.918
13224	+47.49494	-0.24595	0.236	0.960

Table 3—Continued

SN ID	$\alpha_{\text{J}2000}$ [degrees]	$\delta_{\text{J}2000}$ [degrees]	Redshift	Fitprob
13323	-36.94882	-0.13476	0.232	0.303
13432	-41.54678	-1.07564	0.229	0.059
13633	+4.66560	+0.00587	0.388	0.306
13703	+39.01363	+1.25339	0.235	0.952
13864	-11.42593	+0.19101	0.293	0.304
13907	+14.17929	+0.23222	0.198	0.686
13908	+15.91596	+0.29503	0.240	0.010
13933	-22.73453	-0.56346	0.432	0.582
13958	+21.78776	+0.80035	0.303	0.326
14186	-22.14954	+0.99220	0.313	0.241
14317	-44.42935	+0.33021	0.181	0.977
14333	+16.28526	-0.01270	0.271	0.420
14340	-14.17343	-0.85538	0.277	0.432
14524	+41.56276	-0.79787	0.272	0.222
14525	+16.88274	+0.47712	0.155	0.995
14545	-8.25183	+1.01714	0.278	0.423
14589	+48.01208	-0.67760	0.270	0.906
14750	+34.51896	+0.65297	0.215	0.622
14784	-36.20166	-0.34829	0.192	0.717
14961	+15.91944	+0.93097	0.370	0.146

Table 3—Continued

SN ID	$\alpha_{\text{J}2000}$ [degrees]	$\delta_{\text{J}2000}$ [degrees]	Redshift	Fitprob
15033	+15.77839	-0.15672	0.220	0.008
15272	-9.22699	+0.08437	0.280	0.394
15303	-9.49118	+0.54095	0.234	0.009
15343	-36.32767	+0.68477	0.174	0.016
15345	-24.74323	+0.81052	0.280	0.213
15362	-5.27002	+0.76059	0.134	0.043
15381	-52.92377	+0.49337	0.162	0.192
15454	-32.14066	-0.84815	0.383	0.798
15587	+54.41718	+0.99825	0.219	0.947
15675	-16.82639	+0.36414	0.235	0.934
15748	+48.11442	-0.13071	0.157	0.078
15765	+32.84710	+0.24601	0.305	0.706
15784	-3.32635	-0.61540	0.277	0.794
15802	+29.75320	-1.07942	0.342	0.999
15806	+24.09219	-0.83070	0.250	0.569
15823	-45.74744	+0.19901	0.215	0.989
15850	+0.66751	-1.16522	0.250	0.461
15892	-36.80106	+0.68938	0.184	0.194
15909	+11.31475	+0.79673	0.218	0.010
15971	+40.11259	+0.52619	0.316	0.056

Table 3—Continued

SN ID	$\alpha_{\text{J}2000}$ [degrees]	$\delta_{\text{J}2000}$ [degrees]	Redshift	Fitprob
16052	+58.60019	-0.72081	0.144	0.923
16091	+50.19004	+0.84181	0.301	0.996
16103	-47.02484	-1.05017	0.202	0.069
16152	+46.90844	+0.98769	0.272	0.715
16163	+31.49918	-0.85579	0.155	0.204
16462	+17.04058	-0.38646	0.245	0.486
16467	-31.41428	+0.11822	0.221	0.062
16768	-37.29944	+0.69283	0.169	0.084
17206	+45.98524	+0.72816	0.156	0.301
17434	+18.43727	-0.07290	0.179	0.840
17748	+9.80709	-0.27714	0.179	0.971
17882	+15.01838	+1.24641	0.270	0.102
17928	-1.52991	+1.11463	0.197	0.975
17958	+34.43497	-0.71299	0.276	0.377
18047	+22.07419	-0.65805	0.359	0.025
18630	-12.02002	-0.26443	0.359	0.009
18647	-37.10809	-0.30387	0.213	0.389
19525	+23.78299	-0.18406	0.153	0.388
19787	+0.28111	-0.09813	0.197	0.495
19833	+38.87204	-1.17885	0.233	0.034

Table 3—Continued

SN ID	$\alpha_{\text{J}2000}$ [degrees]	$\delta_{\text{J}2000}$ [degrees]	Redshift	Fitprob
20141	-2.45801	-0.52391	0.342	0.647
20171	+3.01303	+0.21357	0.240	0.034
20232	+7.08330	-0.05822	0.217	0.974
20626	+8.47575	-0.59308	0.276	0.313
20721	-36.81519	-0.62219	0.212	0.180
20788	+51.67339	-0.47783	0.394	0.954
20896	+0.72633	+0.93933	0.361	0.740
21024	+43.94143	-0.05122	0.262	0.005

Table 4. SNe with Photometric Redshifts in the Rate Sample

SN ID	$\alpha_{\text{J}2000}$ [degrees]	$\delta_{\text{J}2000}$ [degrees]	Redshift	Redshift Error	Fitprob
822	+40.56070	-0.86217	0.220	0.018	0.090
1342	-13.47260	+0.11688	0.283	0.026	0.962
1403	-0.29614	+0.43188	0.341	0.034	0.112
1658	-2.49557	+0.65006	0.256	0.025	0.836
1899	-36.65695	-0.70642	0.341	0.037	0.005
2784	+28.07526	-0.04169	0.381	0.021	0.488
2855	+16.17518	-0.35642	0.233	0.016	0.978
3206	+13.57741	+0.41816	0.387	0.031	0.003
3368	+44.45594	+1.23082	0.320	0.035	0.831
3417	-45.72394	+0.97825	0.262	0.016	0.413
3506	-23.74936	-0.97821	0.211	0.011	0.963
3945	-13.99094	-0.28307	0.260	0.017	0.070
3975	+29.82097	+0.20364	0.399	0.019	0.002
3983	+7.27582	-0.25663	0.279	0.021	0.220
4028	+11.01385	+1.24247	0.327	0.030	0.724
4044	+33.41526	+1.24086	0.383	0.027	0.395
4079	+29.20663	+0.75403	0.414	0.015	0.078
4360	+19.65592	+0.91577	0.328	0.021	0.932
4455	+52.15621	-0.06056	0.345	0.040	0.001
4558	+29.88546	+0.29007	0.344	0.043	0.501

Table 4—Continued

SN ID	α_{J2000} [degrees]	δ_{J2000} [degrees]	Redshift	Redshift Error	Fitprob
4572	+36.26846	+0.39601	0.386	0.025	0.058
4578	+38.59660	+0.31129	0.341	0.033	0.516
4579	+38.67472	+0.36412	0.406	0.024	0.884
4714	+37.15236	-0.20551	0.435	0.011	0.016
4757	+34.14671	-1.01575	0.416	0.021	0.232
4803	+32.56401	+0.30202	0.398	0.022	0.636
5199	-11.20758	-0.99494	0.248	0.021	0.761
5235	-22.77576	+0.63615	0.253	0.028	0.373
5468	-17.46933	+0.40476	0.277	0.017	0.965
5524	-43.42136	-0.99036	0.299	0.024	0.175
5543	-3.14093	+0.30325	0.330	0.022	0.808
5702	+12.58325	-0.91914	0.222	0.009	0.931
5731	+11.33848	-0.54451	0.376	0.027	0.300
5735	-48.34122	+0.65057	0.229	0.019	0.785
5792	-31.28583	-1.23786	0.226	0.045	0.066
5802	-31.85498	+0.84568	0.270	0.020	0.996
5803	-24.02011	+0.93223	0.285	0.023	0.360
5917	+6.03683	-0.25513	0.254	0.019	0.994
6055	+37.90630	-0.89602	0.404	0.020	0.250
6225	+0.28751	-1.00040	0.333	0.026	0.225

Table 4—Continued

SN ID	α_{J2000} [degrees]	δ_{J2000} [degrees]	Redshift	Redshift Error	Fitprob
6501	-44.84314	+0.13145	0.338	0.024	0.850
6560	-38.55347	+0.84973	0.290	0.031	0.264
6618	+41.91954	+0.96416	0.313	0.015	1.000
6877	+52.50651	+0.62126	0.321	0.013	0.003
6889	-33.28009	+0.90946	0.290	0.032	0.980
6912	-44.26764	-0.64258	0.369	0.041	0.991
7205	+44.10721	+0.69505	0.315	0.014	0.799
7304	+24.83592	-0.65620	0.256	0.013	0.932
7357	-38.36414	-0.36266	0.392	0.029	0.633
7365	-7.68283	+0.57975	0.406	0.023	0.911
7413	+15.04521	+0.47463	0.380	0.031	0.949
7636	-39.14493	+0.11879	0.396	0.021	0.540
7654	+2.47238	+0.96446	0.388	0.019	0.997
7656	+7.75481	+1.01067	0.335	0.046	0.057
7699	+6.23865	-1.21577	0.355	0.024	0.336
7712	+10.95986	-1.24082	0.426	0.015	0.587
7717	+14.44051	-1.23264	0.329	0.025	0.741
7802	-14.42410	+0.72910	0.310	0.026	0.650
7803	-13.91367	+0.69040	0.382	0.032	0.176
7841	+10.31183	-0.05151	0.409	0.022	0.663

Table 4—Continued

SN ID	$\alpha_{\text{J}2000}$ [degrees]	$\delta_{\text{J}2000}$ [degrees]	Redshift	Redshift Error	Fitprob
7884	+21.76736	+0.12340	0.344	0.035	0.991
8092	+50.15116	+0.09387	0.329	0.022	0.696
8118	-4.14130	+0.29712	0.415	0.025	0.658
8138	+11.46659	+0.37805	0.331	0.027	0.816
8226	-25.18280	+0.74912	0.429	0.015	0.654
8297	+24.97450	+0.69145	0.255	0.019	0.799
10559	-5.88357	-1.22660	0.257	0.027	0.696
8700	+35.10958	+0.22706	0.385	0.031	0.510
8705	+40.43310	+0.26872	0.384	0.034	0.336
8793	+11.93775	-0.56470	0.383	0.034	0.023
9052	+21.04114	-0.48308	0.237	0.017	0.887
9109	+26.38895	+0.85063	0.259	0.018	0.921
9132	+16.25518	+0.54001	0.368	0.034	0.715
9218	+46.70148	-0.70051	0.236	0.020	0.060
9334	-13.00699	+0.84164	0.336	0.036	0.242
9632	+30.17027	+1.24947	0.383	0.016	0.691
9895	+35.26586	+0.50430	0.328	0.027	0.385
10113	+54.18169	-0.14042	0.296	0.022	0.985
11092	-57.37665	+1.12162	0.090	0.005	0.711
12936	+32.04546	-1.05151	0.194	0.029	0.567

Table 4—Continued

SN ID	$\alpha_{\text{J}2000}$ [degrees]	$\delta_{\text{J}2000}$ [degrees]	Redshift	Redshift Error	Fitprob
13015	+25.30317	+0.92776	0.225	0.008	0.002
13016	+25.58846	+0.97958	0.244	0.018	0.749
13064	-16.32651	-1.13961	0.228	0.020	0.943
13073	-23.97488	+0.14211	0.323	0.035	0.882
13096	-1.62985	-1.20224	0.363	0.032	0.508
13098	-0.82284	-1.19228	0.276	0.019	0.474
13108	+9.87074	-1.20040	0.288	0.034	0.136
13144	+20.08210	-0.33359	0.275	0.016	0.012
13147	-1.80631	+0.08943	0.370	0.032	0.496
13168	+1.60157	+0.62138	0.337	0.029	0.699
13329	-19.27988	-0.10852	0.319	0.022	0.848
13334	-38.32297	+0.39447	0.364	0.030	0.201
13437	-31.25275	-0.66195	0.379	0.024	0.980
13441	-13.04706	-0.23305	0.282	0.035	0.741
13460	-14.28552	+0.14190	0.299	0.026	0.011
13474	+11.82052	-1.06794	0.328	0.013	0.021
13476	-3.98340	-0.79097	0.310	0.028	0.383
13477	+7.80524	-0.70838	0.407	0.022	0.182
13491	+43.28595	+0.11893	0.372	0.016	0.008
13554	+7.15682	+0.87184	0.332	0.028	0.719

Table 4—Continued

SN ID	α_{J2000} [degrees]	δ_{J2000} [degrees]	Redshift	Redshift Error	Fitprob
13615	-48.58765	+1.18661	0.232	0.021	0.854
13646	-2.52744	-1.03215	0.292	0.016	0.608
13649	-4.47165	-0.61896	0.319	0.027	0.493
13675	-49.34103	-0.91660	0.292	0.022	0.225
13729	-41.08133	+0.87517	0.343	0.041	0.741
13737	-21.07382	+0.96260	0.329	0.029	0.060
13740	-48.78296	-1.08869	0.241	0.018	0.027
13768	-36.92404	-0.76319	0.240	0.016	0.808
13813	-41.67911	-0.40486	0.240	0.016	0.994
13833	-5.67856	-0.20943	0.419	0.019	0.209
13843	-40.83966	+0.20718	0.433	0.012	0.015
13859	+11.06211	+0.96698	0.324	0.021	0.961
13861	-22.15250	+0.07537	0.365	0.028	0.684
13867	-8.54517	+0.02935	0.333	0.038	0.538
13896	+2.71280	-0.06992	0.229	0.015	0.538
13901	+21.92091	-0.14467	0.421	0.017	0.001
13904	+6.85967	+0.28349	0.244	0.015	0.032
13909	+16.41927	+0.31172	0.293	0.011	0.317
13952	+4.63440	+0.78849	0.369	0.041	0.133
14074	-17.87405	-0.82529	0.321	0.028	0.771

Table 4—Continued

SN ID	$\alpha_{\text{J}2000}$ [degrees]	$\delta_{\text{J}2000}$ [degrees]	Redshift	Redshift Error	Fitprob
14093	+26.53920	-1.05637	0.427	0.015	0.205
14206	+17.39464	+0.70405	0.237	0.012	0.579
14231	+57.64965	+0.78754	0.162	0.013	0.964
14268	+52.19934	+0.39107	0.259	0.013	0.870
14304	-48.99826	-0.60592	0.322	0.022	0.771
14322	-6.22708	-0.16948	0.377	0.030	0.603
14343	+0.70710	-0.95408	0.274	0.025	0.665
14347	+16.98071	-1.01713	0.296	0.021	0.348
14357	+47.64600	-0.93812	0.414	0.019	0.183
14361	+43.51542	-0.10534	0.375	0.016	0.950
14372	+50.81182	-0.14131	0.301	0.022	0.778
14403	+16.83825	+0.65173	0.293	0.012	0.114
14438	-19.93484	-1.06933	0.282	0.011	0.470
14444	-23.29849	-0.81572	0.244	0.020	0.339
14453	-43.71375	+0.94936	0.349	0.028	0.305
14463	+3.14527	-0.35054	0.207	0.019	0.981
14467	+25.60195	-0.31297	0.358	0.020	0.810
14470	+44.21490	-0.35178	0.179	0.010	0.998
14522	+28.52871	-0.72565	0.389	0.036	0.828
14528	-10.06488	+0.47960	0.337	0.031	0.543

Table 4—Continued

SN ID	$\alpha_{\text{J}2000}$ [degrees]	$\delta_{\text{J}2000}$ [degrees]	Redshift	Redshift Error	Fitprob
14531	+2.62424	+0.48453	0.356	0.023	0.025
14539	+28.24310	+0.50526	0.379	0.029	0.528
14540	+36.51231	+0.58206	0.257	0.011	0.999
14549	+8.18106	+0.96332	0.229	0.022	0.725
14561	+46.69879	+0.94942	0.214	0.016	0.018
14588	+47.68921	-0.77679	0.372	0.029	0.685
14617	+53.36466	+1.02023	0.258	0.015	0.796
14638	-1.44022	-0.12483	0.331	0.023	0.366
14644	+24.08068	-0.06971	0.405	0.030	0.253
14708	+15.31452	-0.46494	0.337	0.032	0.701
14760	+56.25041	+0.72820	0.321	0.025	0.954
14763	+33.56654	+1.12131	0.351	0.041	0.664
14786	-28.17960	-0.32145	0.321	0.034	0.897
14809	-28.62418	-0.65592	0.311	0.026	0.157
14823	+20.80287	-0.31058	0.279	0.035	0.815
14888	+25.70452	-0.64986	0.366	0.014	0.699
14900	+45.23616	-0.63561	0.432	0.012	0.100
14951	+53.00833	+0.41389	0.427	0.014	0.023
14965	+18.93550	+1.03783	0.238	0.028	0.793
15055	+58.49916	-0.05169	0.196	0.015	1.000

Table 4—Continued

SN ID	$\alpha_{\text{J}2000}$ [degrees]	$\delta_{\text{J}2000}$ [degrees]	Redshift	Redshift Error	Fitprob
15103	-21.90140	-0.50470	0.374	0.031	0.715
15108	+24.43465	-0.54161	0.412	0.018	0.213
15137	-3.89270	-0.80658	0.281	0.021	0.899
15291	-21.91617	-1.15178	0.313	0.030	0.336
15198	+34.62743	-0.21229	0.290	0.008	1.000
15260	-20.82269	-0.27577	0.215	0.016	0.983
15263	-34.19357	+0.00996	0.389	0.031	0.523
15268	-21.55505	+0.13868	0.275	0.019	0.758
15289	-25.56696	-1.19865	0.376	0.022	0.818
15294	-41.52478	-0.73191	0.347	0.046	0.115
15324	+31.69360	-0.83908	0.388	0.017	0.001
15351	-33.46466	-0.05332	0.326	0.047	0.831
15357	-24.66269	+0.23419	0.266	0.026	0.646
15359	-12.54376	+0.31050	0.262	0.018	0.071
15363	+13.03311	+0.66130	0.356	0.038	0.331
15417	+15.55787	+0.46188	0.304	0.027	0.859
15419	+19.90523	+0.88563	0.267	0.021	0.937
15423	+36.50804	+0.62611	0.318	0.014	0.134
15428	+39.09415	+1.04246	0.410	0.014	0.099
15448	+52.38031	-1.14735	0.232	0.016	0.936

Table 4—Continued

SN ID	α_{J2000} [degrees]	δ_{J2000} [degrees]	Redshift	Redshift Error	Fitprob
15455	-29.91956	-1.05142	0.395	0.030	0.389
15483	-40.20804	+0.69697	0.321	0.033	0.901
15489	+7.75260	-0.07103	0.365	0.028	0.996
15496	+8.07390	+0.27446	0.237	0.011	0.949
15511	+44.93024	-0.95519	0.256	0.026	0.993
15525	+51.52761	+1.13072	0.355	0.045	0.729
15553	-38.87988	+0.94418	0.285	0.035	0.935
15592	-39.53268	-1.17850	0.341	0.030	0.090
15777	-33.81146	-0.61831	0.296	0.013	0.405
15785	+30.27846	-0.53928	0.331	0.024	0.172
15710	+55.05272	+0.72199	0.363	0.028	0.609
15719	+37.64792	+1.10330	0.249	0.026	0.612
15726	-10.50537	-0.00728	0.394	0.017	0.124
15745	+42.20790	-0.10763	0.414	0.022	0.941
15751	+54.02817	-0.05176	0.331	0.035	0.784
15782	-7.32382	-0.42804	0.314	0.031	0.058
15812	+19.35990	-0.30902	0.312	0.023	0.300
15814	+29.72514	-0.37273	0.350	0.021	0.971
15816	+19.45456	+0.09876	0.326	0.043	0.110
15817	+29.56453	+0.01327	0.394	0.026	0.306

Table 4—Continued

SN ID	α_{J2000} [degrees]	δ_{J2000} [degrees]	Redshift	Redshift Error	Fitprob
15829	-36.91449	-0.76231	0.322	0.025	0.967
15860	+4.59735	+0.18303	0.288	0.016	0.959
15870	+30.01619	-0.23499	0.396	0.025	0.439
15874	+39.76944	-0.38710	0.410	0.026	0.645
15903	+48.90611	-0.60267	0.283	0.060	0.047
15994	+11.93237	+0.10035	0.243	0.040	0.168
16111	-30.68307	+0.93545	0.230	0.019	0.999
16130	+51.77484	+0.15773	0.325	0.020	0.171
16148	+48.66113	+0.58814	0.308	0.024	0.916
16199	-27.05576	+1.13495	0.232	0.033	0.575
16220	+9.92570	+0.68008	0.314	0.038	0.625
16225	+36.51204	+0.26114	0.390	0.025	0.555
16237	+23.01032	-0.62387	0.296	0.015	0.010
16238	+27.91512	-0.43587	0.339	0.043	0.466
16247	+56.36977	-0.46345	0.311	0.052	0.110
16302	-28.23279	+0.18343	0.187	0.013	0.003
16410	-40.28500	+0.64812	0.309	0.020	0.051
16460	+11.00961	-0.23004	0.286	0.018	0.829
17541	-34.94067	+0.72586	0.261	0.026	0.628
17577	-28.08521	-1.05463	0.283	0.035	0.015

Table 4—Continued

SN ID	α_{J2000} [degrees]	δ_{J2000} [degrees]	Redshift	Redshift Error	Fitprob
17647	+34.28204	-0.80163	0.249	0.012	0.922
17695	+41.98984	+0.58951	0.170	0.014	0.337
17773	+33.28418	-0.30634	0.273	0.021	0.790
17820	+16.13956	-0.46653	0.306	0.021	0.544
17829	+53.03160	-0.83546	0.332	0.037	0.133
17899	-6.30051	-0.15169	0.252	0.027	0.935
17906	+56.23551	+0.40241	0.184	0.012	0.995
17925	-13.69412	+0.30397	0.286	0.020	0.444
17949	+29.20499	-0.23557	0.305	0.020	0.358
17965	-19.17645	-0.75888	0.296	0.034	0.986
18041	+10.89522	-0.69872	0.400	0.021	0.246
18049	+6.31049	-0.36792	0.261	0.021	0.411
18083	+36.34912	-1.20823	0.179	0.029	0.541
18146	+32.42931	-0.00044	0.432	0.016	0.370
18243	-24.95514	-0.74009	0.278	0.023	0.998
18253	-14.41571	-0.90850	0.252	0.049	0.020
18283	+39.75129	-0.54572	0.232	0.038	0.484
18324	+6.38100	+0.79376	0.278	0.036	0.958
18339	+31.87198	+1.15926	0.303	0.021	0.670
18362	+10.13653	-0.18209	0.220	0.028	0.956

Table 4—Continued

SN ID	$\alpha_{\text{J}2000}$ [degrees]	$\delta_{\text{J}2000}$ [degrees]	Redshift	Redshift Error	Fitprob
18374	+2.56478	-0.17714	0.286	0.015	0.999
18405	-46.45111	-0.91769	0.236	0.025	0.950
18479	-12.04922	-0.81114	0.290	0.018	0.571
18582	-51.33374	-0.63135	0.266	0.015	0.718
18588	-21.52823	-1.20459	0.348	0.031	0.559
18589	-19.16541	-1.14140	0.334	0.018	0.130
18651	-27.54291	+0.11260	0.214	0.029	0.875
18666	-17.43558	+0.19474	0.301	0.016	0.992
18704	+11.52182	-0.52672	0.302	0.025	0.557
18801	+49.76012	-0.45803	0.379	0.041	0.770
18824	+23.40139	+1.19070	0.388	0.019	0.428
18884	-33.73700	-0.94996	0.155	0.017	0.001
18920	+53.22518	+0.53269	0.279	0.027	0.588
18942	+17.49710	-0.01868	0.432	0.015	0.379
18943	+20.76962	-0.06722	0.328	0.036	0.762
18947	+11.18694	-0.87064	0.329	0.029	0.306
18952	+11.30682	+0.82777	0.313	0.041	0.152
18971	+31.44543	+1.20877	0.263	0.028	0.648
18990	+15.97268	-0.59233	0.407	0.025	0.726
18993	+24.32056	-0.50393	0.303	0.029	0.299

Table 4—Continued

SN ID	$\alpha_{\text{J}2000}$ [degrees]	$\delta_{\text{J}2000}$ [degrees]	Redshift	Redshift Error	Fitprob
19000	+37.95206	-0.49290	0.271	0.010	0.377
19001	+41.64711	-0.45204	0.271	0.024	0.254
19205	-37.81393	-0.84680	0.313	0.022	0.973
19209	-15.73669	-0.88774	0.163	0.018	0.061
19274	-6.11456	-0.57059	0.328	0.027	0.798
19322	-4.55545	+1.23752	0.311	0.014	0.200
19335	-9.94180	+0.39510	0.323	0.046	0.496
19336	-1.12259	+0.26392	0.386	0.017	0.052
19339	+5.99431	+0.31237	0.319	0.020	0.536
19347	+30.75784	+0.35759	0.294	0.016	0.982
19352	+40.32961	+0.25313	0.334	0.033	0.569
19399	+55.71893	+0.83188	0.251	0.020	0.881
19459	+47.33323	-0.73490	0.136	0.009	0.633
19467	-19.03510	-0.97697	0.302	0.036	0.710
19545	-29.55695	+0.40112	0.243	0.032	0.167
19556	+17.70001	+0.22681	0.344	0.018	0.923
19593	+29.96931	+0.67895	0.307	0.034	0.227
19708	+42.17281	+0.65459	0.165	0.010	0.667
19723	-21.10834	+0.41763	0.260	0.024	0.802
19769	-9.55649	-0.97642	0.200	0.020	0.276

Table 4—Continued

SN ID	$\alpha_{\text{J}2000}$ [degrees]	$\delta_{\text{J}2000}$ [degrees]	Redshift	Redshift Error	Fitprob
19777	-10.91434	-0.50685	0.421	0.022	0.020
19804	+12.21571	-0.21600	0.320	0.016	0.008
19821	-3.22058	+1.02593	0.245	0.026	0.736
19825	+34.63781	+0.88079	0.165	0.014	0.928
19848	+49.42086	+0.90219	0.262	0.033	0.583
19986	+29.62428	+0.15794	0.363	0.028	0.947
19987	+16.04479	-0.32652	0.255	0.015	0.020
20033	+22.93019	-0.73191	0.216	0.021	0.901
20046	-38.50684	+0.80122	0.261	0.019	0.940
20090	-58.10004	-0.07334	0.201	0.018	0.790
20104	-41.86163	+0.28148	0.314	0.022	0.015
20231	+4.58886	-0.03239	0.374	0.016	0.700
20272	+17.21835	-0.02123	0.414	0.023	0.659
20276	+34.56314	-0.11415	0.359	0.024	0.709
20278	+36.89183	-0.18167	0.325	0.024	0.058
20467	+20.01988	+0.91342	0.277	0.022	0.998
20476	-34.57996	+0.83897	0.304	0.016	0.733
20491	-9.01843	-1.19331	0.228	0.019	0.999
20497	+11.45800	-1.18681	0.333	0.026	0.545
20514	+23.07604	-0.75532	0.388	0.022	0.026

Funding for the SDSS and SDSS-II has been provided by the Alfred P. Sloan Foundation, the Participating Institutions, the National Science Foundation (NSF), the U.S. Department of Energy, the National Aeronautics and Space Administration (NASA), the Japanese Monbukagakusho, the Max Planck Society, and the Higher Education Funding Council for England. The SDSS Web Site is <http://www.sdss.org/>.

The SDSS is managed by the Astrophysical Research Consortium for the Participating Institutions. The Participating Institutions are the American Museum of Natural History, Astrophysical Institute Potsdam, University of Basel, University of Cambridge, Case Western Reserve University, University of Chicago, Drexel University, Fermilab, the Institute for Advanced Study, the Japan Participation Group, Johns Hopkins University, the Joint Institute for Nuclear Astrophysics, the Kavli Institute for Particle Astrophysics and Cosmology, the Korean Scientist Group, the Chinese Academy of Sciences (LAMOST), Los Alamos National Laboratory, the Max-Planck-Institute for Astronomy (MPIA), the Max-Planck-Institute for Astrophysics (MPA), New Mexico State University, Ohio State University, University of Pittsburgh, University of Portsmouth, Princeton University, the United States Naval Observatory, and the University of Washington.

This work is based in part on observations made at the following telescopes. The Hobby-Eberly Telescope (HET) is a joint project of the University of Texas at Austin, the Pennsylvania State University, Stanford University, Ludwig-Maximilians-Universität München, and Georg-August-Universität Göttingen. The HET is named in honor of its principal benefactors, William P. Hobby and Robert E. Eberly. The Marcario Low-Resolution Spectrograph is named for Mike Marcario of High Lonesome Optics, who fabricated several optical elements for the instrument but died before its completion; it is a joint project of the Hobby-Eberly Telescope partnership and the Instituto de Astronomía de la Universidad Nacional Autónoma de México. The Apache Point Observatory 3.5 m telescope is owned and operated by the Astrophysical Research Consortium. We thank the observatory director, Suzanne Hawley, and site manager, Bruce Gillespie, for their support of this project. The Subaru Telescope is operated by the National Astronomical Observatory of Japan. The William Herschel Telescope is operated by the Isaac Newton Group, on the island of La Palma in the Spanish Observatorio del Roque de los Muchachos of the Instituto de Astrofísica de Canarias. Based in part on observations made with the Nordic Optical Telescope, operated on the island of La Palma jointly by Denmark, Finland, Iceland, Norway, and Sweden, in the Spanish Observatorio del Roque de los Muchachos of the Instituto de Astrofísica de Canarias. Kitt Peak National Observatory, National Optical Astronomy Observatory, is operated by the Association of Universities for Research in Astronomy (AURA), Inc., under cooperative agreement with the NSF. The W. M. Keck Observatory is operated as a scientific partnership among the California Institute of Technology, the University of California, and NASA; it was made

Table 4—Continued

SN ID	$\alpha_{\text{J}2000}$ [degrees]	$\delta_{\text{J}2000}$ [degrees]	Redshift	Redshift Error	Fitprob
20534	-20.39160	-0.23645	0.286	0.010	0.117
20537	-45.16870	-0.30518	0.338	0.022	0.322
20612	-40.53510	-0.47161	0.343	0.037	0.484
20663	+16.45225	+0.82060	0.295	0.026	0.898
20722	-34.74387	+0.70129	0.295	0.025	0.572
20744	-13.45078	+0.35883	0.233	0.021	0.805
20750	+23.14062	+0.41276	0.291	0.027	0.903
20791	-42.05215	-0.38600	0.319	0.039	0.534
20819	+43.20791	+1.21915	0.318	0.020	0.083
20844	+13.00876	-1.12150	0.406	0.024	0.512
20971	+29.04193	-0.21597	0.293	0.019	0.235
21015	+38.37030	-0.98158	0.376	0.029	0.843
21081	+12.03145	-0.55571	0.323	0.032	0.090
21306	-7.07675	+0.09141	0.315	0.034	0.976

Table 5. SN Rate vs. Redshift

Redshift	SN Rate ^a [10^{-5} SNe yr $^{-1}$ Mpc $^{-3}$ h_{70}^3]	$-\Delta N/N^b$	$N_{\text{CC}}/N_{\text{Ia}}$
0.025 - 0.050	$2.78^{+1.12+0.15}_{-0.83-0.00}$	0.00 %	...
0.075 - 0.125	$2.59^{+0.52+0.18}_{-0.44-0.01}$	-0.06 %	$0.71^{+0.56}_{-0.33}$ %
0.125 - 0.175	$3.07^{+0.38+0.35}_{-0.34-0.05}$	-0.21 %	$2.99^{+2.37}_{-1.40}$ %
0.175 - 0.225	$3.48^{+0.32+0.82}_{-0.30-0.07}$	-0.21 %	$2.71^{+2.14}_{-1.27}$ %
0.225 - 0.275	$3.65^{+0.31+1.82}_{-0.28-0.12}$	+0.28 %	$2.06^{+1.63}_{-0.96}$ %
0.275 - 0.325	$4.34^{+0.37+3.96}_{-0.34-0.16}$	+1.86 %	$0.67^{+0.53}_{-0.31}$ %

^aThe errors given are statistical and systematic, respectively.

^bAssuming a rate model $r_V \propto (1+z)^{2.04}$; see §3.3.

possible by the generous financial support of the W. M. Keck Foundation. Based partially on observations made with the Italian Telescopio Nazionale Galileo (TNG) operated on the island of La Palma by the Fundación Galileo Galilei of the INAF (Istituto Nazionale di Astrofisica) at the Spanish Observatorio del Roque de los Muchachos of the Instituto de Astrofísica de Canarias.

This work was supported in part by the Kavli Institute for Cosmological Physics at the University of Chicago through grants NSF PHY-0114422 and NSF PHY-0551142, and by an endowment from the Kavli Foundation and its founder Fred Kavli. This work was also partially supported by the US Department of Energy through grants DE-FG02-08ER41562 to Rutgers University (PI: S.W.J.) and DE-FG02-08ER41563 to U.C. Berkeley (PI: A.V.F.), as well as by NSF grants AST-0607485 and AST-0908886 (PI: A.V.F.).

REFERENCES

- Alard, C., & Lupton, R. H. 1998, ApJ, 503, 325
- Aldering, G., Antilogus, P., Bailey, S., Baltay, C., Bauer, A., Blanc, N., Bongard, S., Copin, Y., Gangler, E., Gilles, S., Kessler, R., Kocevski, D., Lee, B. C., Loken, S., Nugent, P., Pain, R., Pecontal, E., Pereira, R., Perlmutter, S., Rabinowitz, D., Rigaudier, G., Scalzo, R., Smadja, G., Thomas, R. C., Wang, L., & Weaver, B. A. 2006, ApJ, 650, 510
- Astier, P., Guy, J., Regnault, N., Pain, R., Aubourg, E., Balam, D., Basa, S., Carlberg, R. G., Fabbro, S., Fouchez, D., Hook, I. M., Howell, D. A., Lafoux, H., Neill, J. D., Palanque-Delabrouille, N., Perrett, K., Pritchett, C. J., Rich, J., Sullivan, M., Taillet, R., Aldering, G., Antilogus, P., Arsenijevic, V., Balland, C., Baumont, S., Brioner, J., Courtois, H., Ellis, R. S., Filiol, M., Gonçalves, A. C., Goobar, A., Guide, D., Hardin, D., Lusset, V., Lidman, C., McMahon, R., Mouchet, M., Mourao, A., Perlmutter, S., Ripoche, P., Tao, C., & Walton, N. 2006, A&A, 447, 31
- Barris, B. J., & Tonry, J. L. 2006, ApJ, 637, 427
- Bazin, G., Palanque-Delabrouille, N., Rich, J., Ruhlmann-Kleider, V., Aubourg, E., Le Guillou, L., Astier, P., Balland, C., Basa, S., Carlberg, R. G., Conley, A., Fouchez, D., Guy, J., Hardin, D., Hook, I. M., Howell, D. A., Pain, R., Perrett, K., Pritchett, C. J., Regnault, N., Sullivan, M., Antilogus, P., Arsenijevic, V., Baumont, S., Fabbro, S., Le Du, J., Lidman, C., Mouchet, M., Mourão, A., & Walker, E. S. 2009, A&A, 499, 653

- Blanc, G., Afonso, C., Alard, C., Albert, J. N., Aldering, G., Amadon, A., Andersen, J., Ansari, R., Aubourg, É., Balland, C., Bareyre, P., Beaulieu, J. P., Charlot, X., Conley, A., Coutures, C., Dahlén, T., Derue, F., Fan, X., Ferlet, R., Folatelli, G., Fouqué, P., Garavini, G., Glicenstein, J. F., Goldman, B., Goobar, A., Gould, A., Graff, D., Gros, M., Haissinski, J., Hamadache, C., Hardin, D., Hook, I. M., de Kat, J., Kent, S., Kim, A., Lasserre, T., Le Guillou, L., Lesquoy, É., Loup, C., Magneville, C., Marquette, J. B., Maurice, É., Maury, A., Milsztajn, A., Moniez, M., Mouchet, M., Newberg, H., Nobili, S., Palanque-Delabrouille, N., Perdereau, O., Prévot, L., Rahal, Y. R., Regnault, N., Rich, J., Ruiz-Lapuente, P., Spiro, M., Tisserand, P., Vidal-Madjar, A., Vigroux, L., Walton, N. A., & Zylberajch, S. 2004, *A&A*, 423, 881
- Botticella, M. T., Riello, M., Cappellaro, E., Benetti, S., Altavilla, G., Pastorello, A., Turatto, M., Greggio, L., Patat, F., Valenti, S., Zampieri, L., Harutyunyan, A., Pignata, G., & Taubenberger, S. 2008, *A&A*, 479, 49
- Cappellaro, E., Evans, R., & Turatto, M. 1999, *A&A*, 351, 459
- D'Andrea, C. B., et al. 2010, *ApJ*, 708, 661
- Dahlen, T., Strolger, L.-G., & Riess, A. G. 2008, *ApJ*, 681, 462
- Dahlen, T., Strolger, L.-G., Riess, A. G., Mobasher, B., Chary, R.-R., Conselice, C. J., Ferguson, H. C., Fruchter, A. S., Giavalisco, M., Livio, M., Madau, P., Panagia, N., & Tonry, J. L. 2004, *ApJ*, 613, 189
- Dilday, B., Kessler, R., Frieman, J. A., Holtzman, J., Marriner, J., Miknaitis, G., Nichol, R. C., Romani, R., Sako, M., Bassett, B., Becker, A., Cinabro, D., DeJongh, F., Depoy, D. L., Doi, M., Garnavich, P. M., Hogan, C. J., Jha, S., Konishi, K., Lampeitl, H., Marshall, J. L., McGinnis, D., Prieto, J. L., Riess, A. G., Richmond, M. W., Schneider, D. P., Smith, M., Takanashi, N., Tokita, K., van der Heyden, K., Yasuda, N., Zheng, C., Barentine, J., Brewington, H., Choi, C., Croots, A., Dembicky, J., Harvanek, M., Im, M., Ketzeback, W., Kleinman, S. J., Krzesiński, J., Long, D. C., Malanushenko, E., Malanushenko, V., McMillan, R. J., Nitta, A., Pan, K., Saurage, G., Snedden, S. A., Watters, S., Wheeler, J. C., & York, D. 2008, *ApJ*, 682, 262
- Dilday, B., et al. 2010, in preparation
- Filippenko, A. V. 1997, *ARA&A*, 35, 309
- Filippenko, A. V. 2005, in *White Dwarfs: Cosmological and Galactic Probes*, ed. E. M. Sion, S. Vennes, & H. L. Shipman (Dordrecht: Springer), 97

Förster, F., Wolf, C., Podsiadlowski, P., & Han, Z. 2006, MNRAS, 368, 1893

Freedman, W. L., Burns, C. R., Phillips, M. M., Wyatt, P., Persson, S. E., Madore, B. F., Contreras, C., Folatelli, G., Gonzalez, E. S., Hamuy, M., Hsiao, E., Kelson, D. D., Morrell, N., Murphy, D. C., Roth, M., Stritzinger, M., Sturch, L., Suntzeff, N. B., Astier, P., Balland, C., Bassett, B., Boldt, L., Carlberg, R. G., Conley, A. J., Frieman, J. A., Garnavich, P. M., Guy, J., Hardin, D., Howell, D. A., Kessler, R., Lampeitl, H., Marriner, J., Pain, R., Perrett, K., Regnault, N., Riess, A. G., Sako, M., Schneider, D. P., Sullivan, M., & Wood-Vasey, M. 2009, ApJ, 704, 1036

Frieman, J. A., Bassett, B., Becker, A., Choi, C., Cinabro, D., DeJongh, F., Depoy, D. L., Dilday, B., Doi, M., Garnavich, P. M., Hogan, C. J., Holtzman, J., Im, M., Jha, S., Kessler, R., Konishi, K., Lampeitl, H., Marriner, J., Marshall, J. L., McGinnis, D., Miknaitis, G., Nichol, R. C., Prieto, J. L., Riess, A. G., Richmond, M. W., Romani, R., Sako, M., Schneider, D. P., Smith, M., Takanashi, N., Tokita, K., van der Heyden, K., Yasuda, N., Zheng, C., Adelman-McCarthy, J., Annis, J., Assef, R. J., Barentine, J., Bender, R., Blandford, R. D., Boroski, W. N., Bremer, M., Brewington, H., Collins, C. A., Croots, A., Dembicky, J., Eastman, J., Edge, A., Edmondson, E., Elson, E., Eyler, M. E., Filippenko, A. V., Foley, R. J., Frank, S., Goobar, A., Gueth, T., Gunn, J. E., Harvanek, M., Hopp, U., Ihara, Y., Ivezić, Ž., Kahn, S., Kaplan, J., Kent, S., Ketzeback, W., Kleinman, S. J., Kollatschny, W., Kron, R. G., Krzesiński, J., Lamenti, D., Leloudas, G., Lin, H., Long, D. C., Lucey, J., Lupton, R. H., Malanushenko, E., Malanushenko, V., McMillan, R. J., Mendez, J., Morgan, C. W., Morokuma, T., Nitta, A., Ostman, L., Pan, K., Rockosi, C. M., Romer, A. K., Ruiz-Lapuente, P., Saurage, G., Schlesinger, K., Snedden, S. A., Sollerman, J., Stoughton, C., Stritzinger, M., Subba Rao, M., Tucker, D., Vaisanen, P., Watson, L. C., Watters, S., Wheeler, J. C., Yanny, B., & York, D. 2008, AJ, 135, 338

Fukugita, M., Ichikawa, T., Gunn, J. E., Doi, M., Shimasaku, K., & Schneider, D. P. 1996, AJ, 111, 1748

Gal-Yam, A., Cenko, S. B., Fox, D. B., Leonard, D. C., Moon, D.-S., Sand, D. J., & Soderberg, A. M. 2007, in The Multicolored Landscape of Compact Objects and Their Explosive Origins, ed. T. Di Salvo, et al. (New York: AIP), 297

Gal-Yam, A., Cenko, S. B., Fox, D. W., Leonard, D. C., Moon, D.-S., Sand, D. J., & Soderberg, A. M. 2005, in 1604–2004: Supernovae as Cosmological Lighthouses, ed. M. Turatto, et al. (San Francisco: ASP), 305

Greggio, L. 2005, A&A, 441, 1055

Gunn, J. E., Carr, M., Rockosi, C., Sekiguchi, M., Berry, K., Elms, B., de Haas, E., Ivezić, Ž., Knapp, G., Lupton, R., Pauls, G., Simcoe, R., Hirsch, R., Sanford, D., Wang, S., York, D., Harris, F., Annis, J., Bartozek, L., Boroski, W., Bakken, J., Haldeman, M., Kent, S., Holm, S., Holmgren, D., Petravick, D., Prosapio, A., Rechenmacher, R., Doi, M., Fukugita, M., Shimasaku, K., Okada, N., Hull, C., Siegmund, W., Mannery, E., Blouke, M., Heidtman, D., Schneider, D., Lucinio, R., & Brinkman, J. 1998, AJ, 116, 3040

Gunn, J. E., Siegmund, W. A., Mannery, E. J., Owen, R. E., Hull, C. L., Leger, R. F., Carey, L. N., Knapp, G. R., York, D. G., Boroski, W. N., Kent, S. M., Lupton, R. H., Rockosi, C. M., Evans, M. L., Waddell, P., Anderson, J. E., Annis, J., Barentine, J. C., Bartoszek, L. M., Bastian, S., Bracker, S. B., Brewington, H. J., Briegel, C. I., Brinkmann, J., Brown, Y. J., Carr, M. A., Czarapata, P. C., Drennan, C. C., Dombeck, T., Federwitz, G. R., Gillespie, B. A., Gonzales, C., Hansen, S. U., Harvanek, M., Hayes, J., Jordan, W., Kinney, E., Klaene, M., Kleinman, S. J., Kron, R. G., Kresinski, J., Lee, G., Limmongkol, S., Lindenmeyer, C. W., Long, D. C., Loomis, C. L., McGehee, P. M., Mantsch, P. M., Neilsen, Jr., E. H., Neswold, R. M., Newman, P. R., Nitta, A., Peoples, J. J., Pier, J. R., Prieto, P. S., Prosapio, A., Rivetta, C., Schneider, D. P., Snedden, S., & Wang, S.-i. 2006, AJ, 131, 2332

Hardin, D., Afonso, C., Alard, C., Albert, J. N., Amadon, A., Andersen, J., Ansari, R., Aubourg, É., Bareyre, P., Bauer, F., Beaulieu, J. P., Blanc, G., Bouquet, A., Char, S., Charlot, X., Couchot, F., Coutures, C., Derue, F., Ferlet, R., Glicenstein, J. F., Goldman, B., Gould, A., Graff, D., Gros, M., Haissinski, J., Hamilton, J. C., de Kat, J., Kim, A., Lasserre, T., Lesquoy, É., Loup, C., Magneville, C., Mansoux, B., Marquette, J. B., Maurice, É., Milsztajn, A., Moniez, M., Palanque-Delabrouille, N., Perdereau, O., Prévot, L., Regnault, N., Rich, J., Spiro, M., Vidal-Madjar, A., Vigroux, L., & Zylberajch, S. 2000, A&A, 362, 419

Hicken, M., Wood-Vasey, W. M., Blondin, S., Challis, P., Jha, S., Kelly, P. L., Rest, A., & Kirshner, R. P. 2009, ApJ, 700, 1097

Hogg, D. W., Finkbeiner, D. P., Schlegel, D. J., & Gunn, J. E. 2001, AJ, 122, 2129

Holtzman, J. A., Marriner, J., Kessler, R., Sako, M., Dilday, B., Frieman, J. A., Schneider, D. P., Bassett, B., Becker, A., Cinabro, D., DeJongh, F., Depoy, D. L., Doi, M., Garnavich, P. M., Hogan, C. J., Jha, S., Konishi, K., Lampeitl, H., Marshall, J. L., McGinnis, D., Miknaitis, G., Nichol, R. C., Prieto, J. L., Riess, A. G., Richmond, M. W., Romani, R., Smith, M., Takanashi, N., Tokita, K., van der Heyden, K., Yasuda, N., & Zheng, C. 2008, AJ, 136, 2306

Horesh, A., Poznanski, D., Ofek, E. O., & Maoz, D. 2008, MNRAS, 389, 1871

Ivezić, Ž., Lupton, R. H., Schlegel, D., Boroski, B., Adelman-McCarthy, J., Yanny, B., Kent, S., Stoughton, C., Finkbeiner, D., Padmanabhan, N., Rockosi, C. M., Gunn, J. E., Knapp, G. R., Strauss, M. A., Richards, G. T., Eisenstein, D., Nicinski, T., Kleinman, S. J., Krzesinski, J., Newman, P. R., Snedden, S., Thakar, A. R., Szalay, A., Munn, J. A., Smith, J. A., Tucker, D., & Lee, B. C. 2004, Astronomische Nachrichten, 325, 583

James, F., & Roos, M. 1994, MINUIT, CERN, Geneva

Jha, S., Riess, A. G., & Kirshner, R. P. 2007, ApJ, 659, 122

Kessler, R., et al. 2009, ApJS, 185, 32

Kuznetsova, N., Barbary, K., Connolly, B., Kim, A. G., Pain, R., Roe, N. A., Aldering, G., Amanullah, R., Dawson, K., Doi, M., Fadeyev, V., Fruchter, A. S., Gibbons, R., Goldhaber, G., Goobar, A., Gude, A., Knop, R. A., Kowalski, M., Lidman, C., Morokuma, T., Meyers, J., Perlmutter, S., Rubin, D., Schlegel, D. J., Spadafora, A. L., Stanishev, V., Strovink, M., Suzuki, N., Wang, L., & Yasuda, N. 2008, ApJ, 673, 981

Kuznetsova, N. V., & Connolly, B. M. 2007, ApJ, 659, 530

Li, W., et al. 2010a, submitted

Li, W., et al. 2010b, submitted

Lupton, R. H., Gunn, J. E., & Szalay, A. S. 1999, AJ, 118, 1406

Madgwick, D. S., Hewett, P. C., Mortlock, D. J., & Wang, L. 2003, ApJ, 599, L33

Neill, J. D., Sullivan, M., Balam, D., Pritchett, C. J., Howell, D. A., Perrett, K., Astier, P., Aubourg, E., Basa, S., Carlberg, R. G., Conley, A., Fabbro, S., Fouchez, D., Guy, J., Hook, I., Pain, R., Palanque-Delabrouille, N., Regnault, N., Rich, J., Taillet, R., Aldering, G., Antilogus, P., Arsenijevic, V., Balland, C., Baumont, S., Brionder, J., Ellis, R. S., Filiol, M., Gonçalves, A. C., Hardin, D., Kowalski, M., Lidman, C., Lusset, V., Mouchet, M., Mourao, A., Perlmutter, S., Ripoche, P., Schlegel, D., & Tao, C. 2006, AJ, 132, 1126

Oyaizu, H., Lima, M., Cunha, C. E., Lin, H., & Frieman, J. 2008, ApJ, 689, 709

Pain, R., Fabbro, S., Sullivan, M., Ellis, R. S., Aldering, G., Astier, P., Deustua, S. E., Fruchter, A. S., Goldhaber, G., Goobar, A., Groom, D. E., Hardin, D., Hook, I. M., Howell, D. A., Irwin, M. J., Kim, A. G., Kim, M. Y., Knop, R. A., Lee, J. C., Lidman, C., McMahon, R. G., Nugent, P. E., Panagia, N., Pennypacker, C. R., Perlmutter, S., Ruiz-Lapuente, P., Schahmaneche, K., Schaefer, B., & Walton, N. A. 2002, ApJ, 577, 120

Perlmutter, S., Aldering, G., Goldhaber, G., Knop, R. A., Nugent, P., Castro, P. G., Deustua, S., Fabbro, S., Goobar, A., Groom, D. E., Hook, I. M., Kim, A. G., Kim, M. Y., Lee, J. C., Nunes, N. J., Pain, R., Pennypacker, C. R., Quimby, R., Lidman, C., Ellis, R. S., Irwin, M., McMahon, R. G., Ruiz-Lapuente, P., Walton, N., Schaefer, B., Boyle, B. J., Filippenko, A. V., Matheson, T., Fruchter, A. S., Panagia, N., Newberg, H. J. M., & Couch, W. J. 1999, ApJ, 517, 565

Phillips, M. M. 1993, ApJ, 413, L105

Poznanski, D., Maoz, D., & Gal-Yam, A. 2007, AJ, 134, 1285

Prieto, J. L., Garnavich, P. M., Phillips, M. M., DePoy, D. L., Parrent, J., Pooley, D., Dwarkadas, V. V., Baron, E., Bassett, B., Becker, A., Cinabro, D., DeJongh, F., Dilday, B., Doi, M., Frieman, J. A., Hogan, C. J., Holtzman, J., Jha, S., Kessler, R., Konishi, K., Lampeitl, H., Marriner, J., Marshall, J. L., Miknaitis, G., Nichol, R. C., Riess, A. G., Richmond, M. W., Romani, R., Sako, M., Schneider, D. P., Smith, M., Takanashi, N., Tokita, K., van der Heyden, K., Yasuda, N., Zheng, C., Wheeler, J. C., Barentine, J., Dembicky, J., Eastman, J., Frank, S., Ketzeback, W., McMillan, R. J., Morrell, N., Folatelli, G., Contreras, C., Burns, C. R., Freedman, W. L., Gonzalez, S., Hamuy, M., Krzeminski, W., Madore, B. F., Murphy, D., Persson, S. E., Roth, M., & Suntzeff, N. B. 2007, astro-ph/0706.4088

Pskovskii, Yu. P. 1977, Soviet Astronomy, 21, 675

Richardson, D., Branch, D., & Baron, E. 2006, AJ, 131, 2233

Richardson, D., Branch, D., Casebeer, D., Millard, J., Thomas, R. C., & Baron, E. 2002, AJ, 123, 745

Riess, A. G., Filippenko, A. V., Challis, P., Clocchiatti, A., Diercks, A., Garnavich, P. M., Gilliland, R. L., Hogan, C. J., Jha, S., Kirshner, R. P., Leibundgut, B., Phillips, M. M., Reiss, D., Schmidt, B. P., Schommer, R. A., Smith, R. C., Spyromilio, J., Stubbs, C., Suntzeff, N. B., & Tonry, J. 1998, AJ, 116, 1009

- Riess, A. G., Strolger, L.-G., Tonry, J., Casertano, S., Ferguson, H. C., Mobasher, B., Challis, P., Filippenko, A. V., Jha, S., Li, W., Chornock, R., Kirshner, R. P., Leibundgut, B., Dickinson, M., Livio, M., Giavalisco, M., Steidel, C. C., Benítez, T., & Tsvetanov, Z. 2004, *ApJ*, 607, 665
- Riess, A. G., Strolger, L.-G., Casertano, S., Ferguson, H. C., Mobasher, B., Gold, B., Challis, P. J., Filippenko, A. V., Jha, S., Li, W., Tonry, J., Foley, R., Kirshner, R. P., Dickinson, M., MacDonald, E., Eisenstein, D., Livio, M., Younger, J., Xu, C., Dahlén, T., & Stern, D. 2007, *ApJ*, 659, 98
- Riess, A. G., Macri, L., Li, W., Lampeitl, H., Casertano, S., Ferguson, H. C., Filippenko, A. V., Jha, S. W., Chornock, R., Greenhill, L., Mutchler, M., Ganeshalingham, M., & Hicken, M. 2009, *ApJS*, 183, 109
- Sako, M., Bassett, B., Becker, A., Cinabro, D., DeJongh, F., Depoy, D. L., Dilday, B., Doi, M., Frieman, J. A., Garnavich, P. M., Hogan, C. J., Holtzman, J., Jha, S., Kessler, R., Konishi, K., Lampeitl, H., Marriner, J., Miknaitis, G., Nichol, R. C., Prieto, J. L., Riess, A. G., Richmond, M. W., Romani, R., Schneider, D. P., Smith, M., Subba Rao, M., Takanashi, N., Tokita, K., van der Heyden, K., Yasuda, N., Zheng, C., Barentine, J., Brewington, H., Choi, C., Dembicky, J., Harnavek, M., Ihara, Y., Im, M., Ketzeback, W., Kleinman, S. J., Krzesiński, J., Long, D. C., Malanushenko, E., Malanushenko, V., McMillan, R. J., Morokuma, T., Nitta, A., Pan, K., Saurage, G., & Snedden, S. A. 2008, *AJ*, 135, 348
- Schechter, P. L., Mateo, M., & Saha, A. 1993, *PASP*, 105, 1342
- Smith, J. A., Tucker, D. L., Kent, S., Richmond, M. W., Fukugita, M., Ichikawa, T., Ichikawa, S.-i., Jorgensen, A. M., Uomoto, A., Gunn, J. E., Hamabe, M., Watanabe, M., Tolea, A., Henden, A., Annis, J., Pier, J. R., McKay, T. A., Brinkmann, J., Chen, B., Holtzman, J., Shimasaku, K., & York, D. G. 2002, *AJ*, 123, 2121
- Smith, M., et al. 2010, in preparation
- Stoughton, C., Lupton, R. H., Bernardi, M., Blanton, M. R., Burles, S., Castander, F. J., Connolly, A. J., Eisenstein, D. J., Frieman, J. A., Hennessy, G. S., Hindsley, R. B., Ivezić, Ž., Kent, S., Kunszt, P. Z., Lee, B. C., Meiksin, A., Munn, J. A., Newberg, H. J., Nichol, R. C., Nicinski, T., Pier, J. R., Richards, G. T., Richmond, M. W., Schlegel, D. J., Smith, J. A., Strauss, M. A., SubbaRao, M., Szalay, A. S., Thakar, A. R., Tucker, D. L., Vanden Berk, D. E., Yanny, B., Adelman, J. K., Anderson, Jr., J. E., Anderson, S. F., Annis, J., Bahcall, N. A., Bakken, J. A., Bartelmann, M., Bastian, S., Bauer, A., Berman, E., Böhringer, H., Boroski, W. N., Bracker,

S., Briegel, C., Briggs, J. W., Brinkmann, J., Brunner, R., Carey, L., Carr, M. A., Chen, B., Christian, D., Colestock, P. L., Crocker, J. H., Csabai, I., Czarapata, P. C., Dalcanton, J., Davidsen, A. F., Davis, J. E., Dehnen, W., Dodelson, S., Doi, M., Dombeck, T., Donahue, M., Ellman, N., Elms, B. R., Evans, M. L., Eyer, L., Fan, X., Federwitz, G. R., Friedman, S., Fukugita, M., Gal, R., Gillespie, B., Glazebrook, K., Gray, J., Grebel, E. K., Greenawalt, B., Greene, G., Gunn, J. E., de Haas, E., Haiman, Z., Haldeman, M., Hall, P. B., Hamabe, M., Hansen, B., Harris, F. H., Harris, H., Harvanek, M., Hawley, S. L., Hayes, J. J. E., Heckman, T. M., Helmi, A., Henden, A., Hogan, C. J., Hogg, D. W., Holmgren, D. J., Holtzman, J., Huang, C.-H., Hull, C., Ichikawa, S.-I., Ichikawa, T., Johnston, D. E., Kauffmann, G., Kim, R. S. J., Kimball, T., Kinney, E., Klaene, M., Kleinman, S. J., Klypin, A., Knapp, G. R., Korienek, J., Krolik, J., Kron, R. G., Krzesiński, J., Lamb, D. Q., Leger, R. F., Limmongkol, S., Lindenmeyer, C., Long, D. C., Loomis, C., Loveday, J., MacKinnon, B., Mannery, E. J., Mantsch, P. M., Margon, B., McGehee, P., McKay, T. A., McLean, B., Menou, K., Merelli, A., Mo, H. J., Monet, D. G., Nakamura, O., Narayanan, V. K., Nash, T., Neilsen, Jr., E. H., Newman, P. R., Nitta, A., Odenkirchen, M., Okada, N., Okamura, S., Ostriker, J. P., Owen, R., Pauls, A. G., Peoples, J., Peterson, R. S., Petravick, D., Pope, A., Pordes, R., Postman, M., Prosapio, A., Quinn, T. R., Rechenmacher, R., Rivetta, C. H., Rix, H.-W., Rockosi, C. M., Rosner, R., Ruthmansdorfer, K., Sandford, D., Schneider, D. P., Scranton, R., Sekiguchi, M., Sergey, G., Sheth, R., Shimasaku, K., Smee, S., Snedden, S. A., Stebbins, A., Stubbs, C., Szapudi, I., Szkody, P., Szokoly, G. P., Tabachnik, S., Tsvetanov, Z., Uomoto, A., Vogeley, M. S., Voges, W., Waddell, P., Walterbos, R., Wang, S.-i., Watanabe, M., Weinberg, D. H., White, R. L., White, S. D. M., Wilhite, B., Wolfe, D., Yasuda, N., York, D. G., Zehavi, I., & Zheng, W. 2002, AJ, 123, 485

Sullivan, M., Howell, D. A., Perrett, K., Nugent, P. E., Astier, P., Aubourg, E., Balam, D., Basa, S., Carlberg, R. G., Conley, A., Fabbro, S., Fouchez, D., Guy, J., Hook, I., Lafoux, H., Neill, J. D., Pain, R., Palanque-Delabrouille, N., Pritchett, C. J., Regnault, N., Rich, J., Taillet, R., Aldering, G., Baumont, S., Bröder, J., Filoli, M., Knop, R. A., Perlmutter, S., & Tao, C. 2006a, AJ, 131, 960

Sullivan, M., Le Borgne, D., Pritchett, C. J., Hodsman, A., Neill, J. D., Howell, D. A., Carlberg, R. G., Astier, P., Aubourg, E., Balam, D., Basa, S., Conley, A., Fabbro, S., Fouchez, D., Guy, J., Hook, I., Pain, R., Palanque-Delabrouille, N., Perrett, K., Regnault, N., Rich, J., Taillet, R., Baumont, S., Bröder, J., Ellis, R. S., Filoli, M., Lusset, V., Perlmutter, S., Ripoche, P., & Tao, C. 2006b, ApJ, 648, 868

Tonry, J. L., Schmidt, B. P., Barris, B., Candia, P., Challis, P., Clocchiatti, A., Coil, A. L.,

Filippenko, A. V., Garnavich, P., Hogan, C., Holland, S. T., Jha, S., Kirshner, R. P., Krisciunas, K., Leibundgut, B., Li, W., Matheson, T., Phillips, M. M., Riess, A. G., Schommer, R., Smith, R. C., Sollerman, J., Spyromilio, J., Stubbs, C. W., & Suntzeff, N. B. 2003, ApJ, 594, 1

Tucker, D. L., Kent, S., Richmond, M. W., Annis, J., Smith, J. A., Allam, S. S., Rodgers, C. T., Stute, J. L., Adelman-McCarthy, J. K., Brinkmann, J., Doi, M., Finkbeiner, D., Fukugita, M., Goldston, J., Greenway, B., Gunn, J. E., Hendry, J. S., Hogg, D. W., Ichikawa, S.-I., Ivezić, Ž., Knapp, G. R., Lampeitl, H., Lee, B. C., Lin, H., McKay, T. A., Merrelli, A., Munn, J. A., Neilsen, Jr., E. H., Newberg, H. J., Richards, G. T., Schlegel, D. J., Stoughton, C., Uomoto, A., & Yanny, B. 2006, Astronomische Nachrichten, 327, 821

Wood-Vasey, W. M., Miknaitis, G., Stubbs, C. W., Jha, S., Riess, A. G., Garnavich, P. M., Kirshner, R. P., Aguilera, C., Becker, A. C., Blackman, J. W., Blondin, S., Challis, P., Clocchiatti, A., Conley, A., Covarrubias, R., Davis, T. M., Filippenko, A. V., Foley, R. J., Garg, A., Hicken, M., Krisciunas, K., Leibundgut, B., Li, W., Matheson, T., Miceli, A., Narayan, G., Pignata, G., Prieto, J. L., Rest, A., Salvo, M. E., Schmidt, B. P., Smith, R. C., Sollerman, J., Spyromilio, J., Tonry, J. L., Suntzeff, N. B., & Zenteno, A. 2007, ApJ, 666, 694

York, D. G., Adelman, J., Anderson, Jr., J. E., Anderson, S. F., Annis, J., Bahcall, N. A., Bakken, J. A., Barkhouser, R., Bastian, S., Berman, E., Boroski, W. N., Bracker, S., Briegel, C., Briggs, J. W., Brinkmann, J., Brunner, R., Burles, S., Carey, L., Carr, M. A., Castander, F. J., Chen, B., Colestock, P. L., Connolly, A. J., Crocker, J. H., Csabai, I., Czarapata, P. C., Davis, J. E., Doi, M., Dombeck, T., Eisenstein, D., Ellman, N., Elms, B. R., Evans, M. L., Fan, X., Federwitz, G. R., Fiscelli, L., Friedman, S., Frieman, J. A., Fukugita, M., Gillespie, B., Gunn, J. E., Gurbani, V. K., de Haas, E., Haldeman, M., Harris, F. H., Hayes, J., Heckman, T. M., Hennessy, G. S., Hindsley, R. B., Holm, S., Holmgren, D. J., Huang, C.-h., Hull, C., Husby, D., Ichikawa, S.-I., Ichikawa, T., Ivezić, Ž., Kent, S., Kim, R. S. J., Kinney, E., Klaene, M., Kleinman, A. N., Kleinman, S., Knapp, G. R., Korienek, J., Kron, R. G., Kunszt, P. Z., Lamb, D. Q., Lee, B., Leger, R. F., Limmongkol, S., Lindenmeyer, C., Long, D. C., Loomis, C., Loveday, J., Lucinio, R., Lupton, R. H., MacKinnon, B., Mannery, E. J., Mantsch, P. M., Margon, B., McGehee, P., McKay, T. A., Meiksin, A., Merelli, A., Monet, D. G., Munn, J. A., Narayanan, V. K., Nash, T., Neilsen, E., Neswold, R., Newberg, H. J., Nichol, R. C., Nicinski, T., Nonino, M., Okada, N., Okamura, S., Ostriker, J. P., Owen, R., Pauls, A. G., Peoples, J., Peterson, R. L., Petracick, D., Pier, J. R., Pope, A., Pordes, R., Prosapio, A., Rechenmacher, R.,

Quinn, T. R., Richards, G. T., Richmond, M. W., Rivetta, C. H., Rockosi, C. M., Ruthmansdorfer, K., Sandford, D., Schlegel, D. J., Schneider, D. P., Sekiguchi, M., Sergey, G., Shimasaku, K., Siegmund, W. A., Smee, S., Smith, J. A., Snedden, S., Stone, R., Stoughton, C., Strauss, M. A., Stubbs, C., SubbaRao, M., Szalay, A. S., Szapudi, I., Szokoly, G. P., Thakar, A. R., Tremonti, C., Tucker, D. L., Uomoto, A., Vanden Berk, D., Vogeley, M. S., Waddell, P., Wang, S.-i., Watanabe, M., Weinberg, D. H., Yanny, B., & Yasuda, N. 2000, AJ, 120, 1579

Zheng, C., Romani, R. W., Sako, M., Marriner, J., Bassett, B., Becker, A., Choi, C., Cinabro, D., DeJongh, F., Depoy, D. L., Dilday, B., Doi, M., Frieman, J. A., Garnavich, P. M., Hogan, C. J., Holtzman, J., Im, M., Jha, S., Kessler, R., Konishi, K., Lampeitl, H., Marshall, J. L., McGinnis, D., Miknaitis, G., Nichol, R. C., Prieto, J. L., Riess, A. G., Richmond, M. W., Schneider, D. P., Smith, M., Takanashi, N., Tokita, K., van der Heyden, K., Yasuda, N., Assef, R. J., Barentine, J., Bender, R., Blandford, R. D., Bremer, M., Brewington, H., Collins, C. A., Crotts, A., Dembicky, J., Eastman, J., Edge, A., Elson, E., Eyler, M. E., Filippenko, A. V., Foley, R. J., Frank, S., Goobar, A., Harvanek, M., Hopp, U., Ihara, Y., Kahn, S., Ketzeback, W., Kleinman, S. J., Kollatschny, W., Krzesiński, J., Leloudas, G., Long, D. C., Lucey, J., Malanushenko, E., Malanushenko, V., McMillan, R. J., Morgan, C. W., Morokuma, T., Nitta, A., Ostman, L., Pan, K., Romer, A. K., Saurage, G., Schlesinger, K., Snedden, S. A., Sollerman, J., Stritzinger, M., Watson, L. C., Watters, S., Wheeler, J. C., & York, D. 2008, AJ, 135, 1766

Zwicky, F. 1938, ApJ, 88, 529